Manuscript No.: acp-2018-574

Title: Marine boundary layer aerosol in Eastern North Atlantic: seasonal variations and key controlling processes

We thank the anonymous referees for their valuable and constructive comments/suggestions on our manuscript. We have revised the manuscript accordingly and please find our point-to-point responses below.

Comments by Anonymous Referee #1:

General Comments:

The paper provides a thorough analysis of the processes controlling the number concentration of the Aitken, accumulation, and sea spray aerosol modes in the eastern North Atlantic based on a several year data record from a site in the Azores. The conclusions that the free troposphere is a significant source of the Aitken and accumulation modes in the MBL and that sea spray aerosol makes up a small fraction of the total particle number at this site are significant and consistent with recently published papers. One intriguing result, if I am interpreting the analysis correctly, is that a significant impact of biogenic sulfur on the CCN population requires the flux of continental Aitken mode particles from the FT to the MBL.

Detailed Comments:

1. Page 2, line 40: add the qualifier ": : :.long term observation IN THE ENA."

Responses: The expression has been corrected as suggested.

2. Page 4, line 3: change to ": : :the parameters of which ARE DERIVED from fitting"?

Responses: The expression has been corrected as suggested.

3. Page 4, line 35: The red trajectories in Fig.1 a, c, and d are all very similar, i.e., originating over the Arctic and passing over northern Canada. Why are they described as "air masses influenced by anthropogenic emissions from North America for fall and winter" and "contribution from Arctic" for Spring. Also – I don't see the "northern Europe air masses" in the trajectories for spring.

Responses:

The trajectories shown in Fig. 1 are average trajectories for each cluster. The individual trajectories are shown in Fig. R1. We've also added this figure as Fig. S3 in the updated SI, and referenced in the manuscript accordingly (see Page 5, Line 1-4).

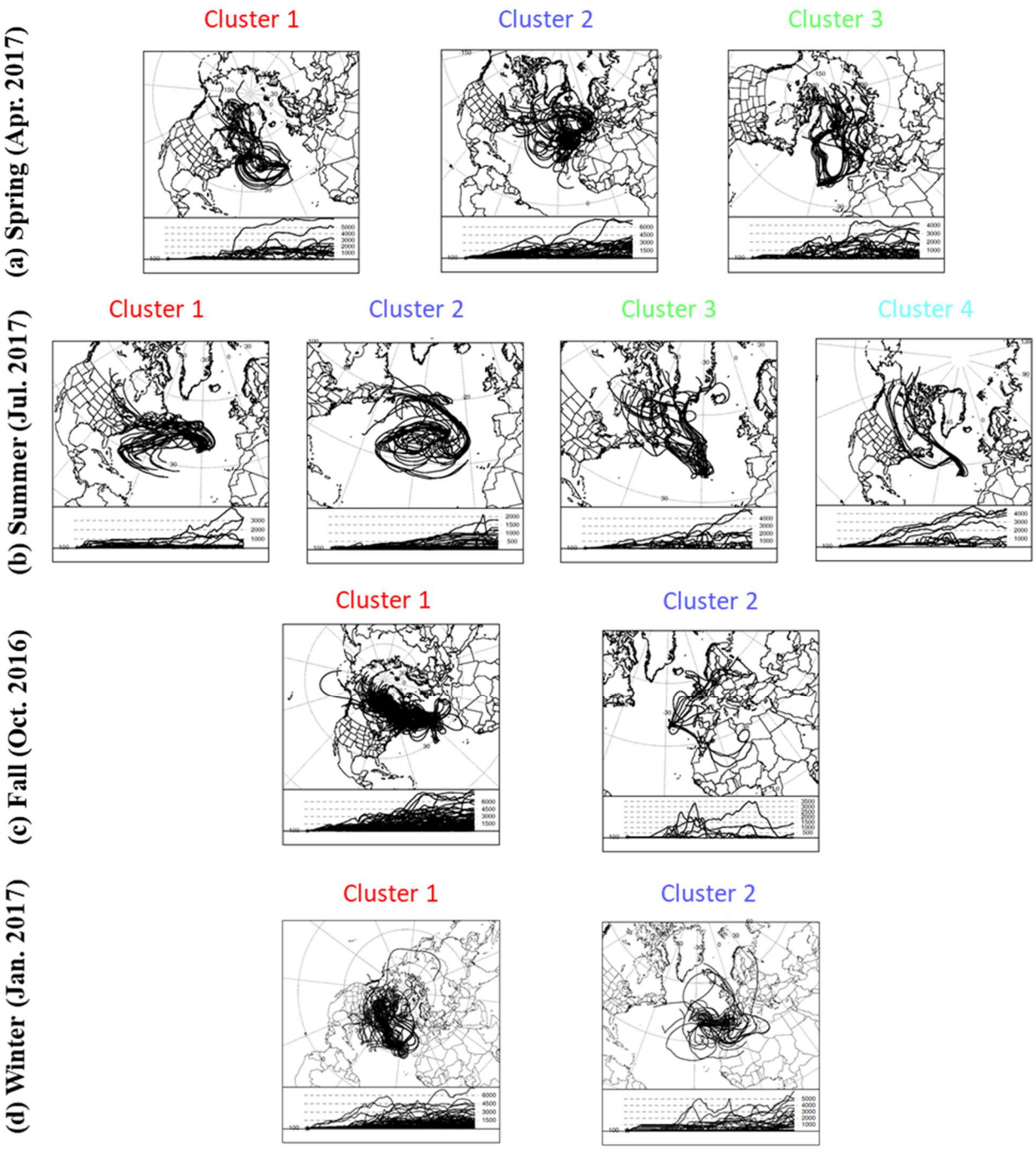

Fig. R1 *(added as Figure S3 in updated SI)* **Detailed trajectories for each cluster shown in Fig. 1.**

4. Figure 3.b2. and throughout: Figure 3.b2. clearly shows that what is termed here to be "Large Accumulation" mode is actually the sea spray aerosol coarse mode. To be in line with what it actually is and with published literature, it would be more appropriate to call it the SSA, PMA (primary marine aerosol), or primary aerosol mode.

Responses:

We agree, as shown in the Fig. 3b2, that the "Large Accumulation" mode is dominated by SSA and is essentially the sea spray aerosol coarse mode under vast majority of the cases. On the other hand, we don't want to simply call the mode "SSA" or "PMA" mode, without presenting any evidence to demonstrate the case (as shown in Fig. 6). We also note during some episodes (not shown in the manuscript), aged biomass burning aerosol and dust likely also contributed substantially to the large accumulation mode. We have added one sentence following the figure as (see Page 6, Line 26-28):

"Based on the average volume size distributions (Fig. 3b2), the "large accumulation mode" is essentially the sea spray aerosol coarse mode under vast majorities of the conditions."

5. Page 6, lines 23 – 24: The Ac mode Dp is 161 +/- 25 in summer and 155 +/- 31 in winter. Does the Ac mode really have a larger Dp in summer than winter given the fairly large standard deviations of the mean Dp?

Responses:

The standard deviation represents the variation of mode diameter during each season. We note that the mean, median, 25th and 75th percentiles of the Ac mode diameter all exhibit a higher value during the summer than that during winter (Fig. R2). The larger mode diameter is also evidenced by the seasonal average size distribution (Fig. 3a). We have modified the sentence to the following (see Page 6, Line 31-32):

"While there is substantial variation within each season, on average, the Ac mode exhibits higher number concentration, larger mode D_p, and higher occurrence in summer than in winter (Table 2)."

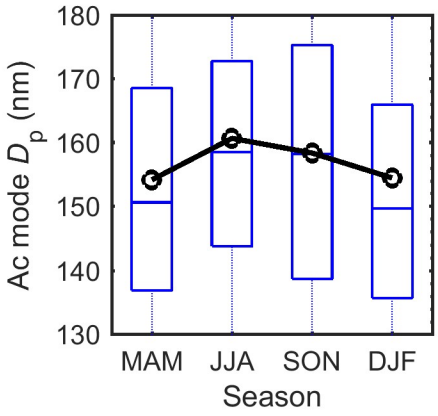

Fig. R2 Seasonal variation of Ac mode diameters.

6. Table 1: There is no instrument listed for MBL height or precipitation rate – unless they are included in the "Vertically pointing K-band: : :." list of instruments.

Responses: They are indeed included in the "Vertically …" list. We've added some solid lines to Table 1 to make it clearer.

7. Table 2: Why aren't modal volumes included in the table – especially since they are referred to in the text (e.g., page 6, line 25).

Responses: The modal volume information are added to Table 2 as suggested. In accordance with the data, we also modified the statement into (see Page 6, Line 34):

"In contrast, LA mode shows opposite seasonal trends, with the number and volume concentrations in winter exceeded 1.5 times those in summer (Table 2)."

8. Page 11, Line 9: should be Figure 6c.

Responses: Fig. 6c was discussed later (Page 11, Line 14). Here we are indeed discussing about Fig. 6b.

9. Page 11, Lines 10 – 12: Has a volume mode with a diameter of 0.6 to 0.8 um ever been observed in the remote marine boundary layer? It is not clear why it is discussed here as a possibility and why the "LA" mode is not simply called the "SSA" mode.

Responses:

Given the prevalence of marine low clouds, the brief discussion here is simply to eliminate the possibility that large accumulation mode observed is a result of in-cloud production of sulfate and/or organics (Pandis et al., 1990; Meng and Seinfeld, 1994; Seinfeld and Pandis, 2016). We agree the "LA" is essentially sea spray aerosol coarse mode under vast majorities of the conditions. Please also see the response to comment #4.

10. Page 11, Lines 15 – 16: There are many, many published papers that establish that MBL supermicron particles are dominated by SSA. Why is it being ebated/emphasized here?

Responses:

Here we're not emphasizing that supermicron particles are dominated by SSA. On the contrary, we are using that as a premise. What we stated is that since LA mode (D_p ~300 to 1000 nm) share the same source with supermicron aerosols (D_p 1~10 μm), and since supermicron aerosols are dominated by SSA in remote MBL, thus we speculate that LA mode should also be dominated by SSA. We've rephrased the description to avoid such confusion as (see Page 11, Line 14-19):

"This is also supported by the strong correlation between V_{LA} and PM_c B_{sca} (Fig. 6c). The PM_c B_{sca} is a surrogate for the supermicron mode (PM_c, D_p 1~10 μm) volume concentration (section 2.2), while supermicron particles are dominated by SSA in remote MBL (Campuzano-Jost et al., 2003). Therefore, the strong correlation suggests that LA particles are also dominated by SSA."

11. Page 12, Lines 7 – 8: There is no need to invoke a lack of correlation of Nat or Nac with wind speed to conclude that SSA is a minor contribution to those two modes. Figure 3 is evidence enough.

Responses:

Fig. 3 does show the fitted LA mode has a minor contribution to At mode or AC mode size range. However, LA mode likely presents the coarse mode of the SSA, and many studies have suggested that source function of SSA extends down to Aitken mode size range. We think lack of correlation provide additional evidence for the minor contribution.

12. Figure 8: Should make it clear in the caption that "(0.1%)" refers to supersaturation level.

Responses: The expression has been corrected as suggested into (see Caption of Fig. 8):

"Figure 8. Estimation of SSA contributions to *CN* and *CCN* (0.1%), namely CCN concentration at 0.1% supersaturation level."

13. Page 12, Line 33: should be ": : :fraction is consistent", not "in consistent".

Responses: The expression has been corrected as suggested.

14. Page 13, Line 2: "The SSA number concentration: : :" What number concentration is being referred to here? The present paper or Quinn et al., 2017?

Responses:

Here we mean the derived number concentration following the approach in Quinn et al. (2017). The sentence has been changed into (see Page 13, Line 2-3):

"In that study, the size distribution of SSA was derived by fitting aerosol size distribution. If we follow the same approach (Quinn et al., 2017), the estimated SSA number concentration is actually N_{LA} shown in this study, which represents 19 % of *CCN* (0.1 %)."

15. Page 13, Lines 3 – 7: Please clarify what the "above estimation" is. Numbering the equations and referring to them by number would help. Also, please define the f_ac,SSA and f_at,SSA terms. Are these the flux of SSA in the accumulation and Aitken modes, respectively?

Responses:

The sentence has been changed into (see Page 13, Line 5-9):

"Based on the estimated SSA contribution to *CN* and *CCN* (Eq. 8a and 8b), we can further estimate the SSA contribution to N_{Ac} and N_{At}, $f_{Ac,\,SSA}$ and $f_{At,\,SSA}$, as:

$$f_{Ac,SSA} = (CCN(0.1\%)_{SSA} - N_{LA}) / N_{Ac}$$
$$f_{At,SSA} = (CN_{SSA} - CCN(0.1\%)_{SSA}) / N_{At}$$

and the corresponding annual mean $f_{Ac,\,SSA}$ and $f_{At,\,SSA}$ are 21 % and 10 %, respectively (Table 4)."

16. Page 14, Lines 13 - 14: Please provide previously published fluxes of DMS in the ENA compared to the remote Southern Ocean. Also – this sentence is incomplete.

Responses:

This sentence is based on Plate 2 in Kettle et al. (1999), so we can only give an estimated range. We've modified the expression into (Page 14, Line 9-11):

"Such difference is likely due to the much higher DMS sea surface concentration in ENA (~7.5 nM) than that in southern oceans (~2.5 nM) (Kettle et al., 1999), or due to the difference between observed and model-simulated aerosol size distributions, etc.."

17. Figure 9: What is meant by secondary processing rate? Isn't the SSA flux a primary process, i.e., direct mechanical production?

Responses: The word "secondary" is deleted throughout.

18. Figure 9b: This half of Figure 9 does not appear to be explained in the main text.

Responses: It was discussed in the second but last paragraph in section 6.2 (Page 14, Line 1-4), and section 6.3. We also added the citation in section 6.3 as (see Page 14, Line 20):

"$\partial_t N_{At}|_{FT}$ is higher in spring-summer while lower in fall-winter, and such seasonal variation is somewhat different from those of CO mixing ratio and EBC mass concentrations (Fig. 9b)."

19. Figure S5: Please provide r^2 values for these correlations to support the conclusion given on page 15, lines 20 – 21.

Responses: The values are added to Fig. S5 (see Fig. R3 below).

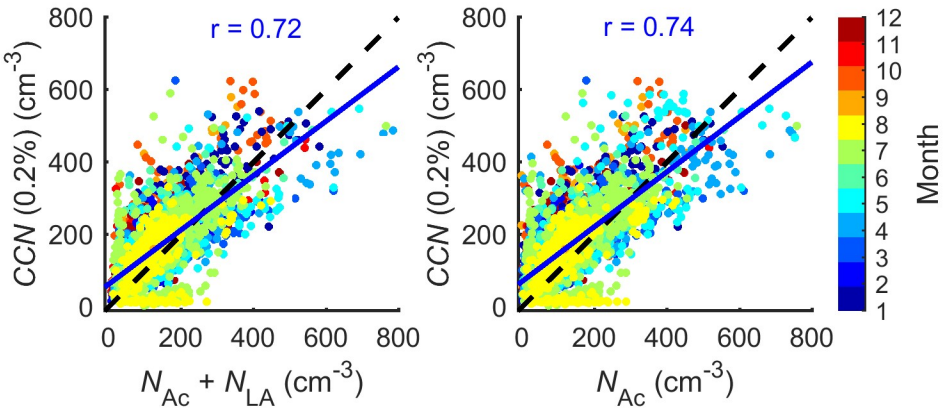

Figure R3. *(Fig. S6 in updated SI)* **Comparison of observed *CCN* concentrations with relevant modal number concentrations.** The black dash line is the 1:1 line shown for reference. The value of *r* given referred to the Pearson correlation coefficient, while the regression line based on York et al. (2004) is also shown for reference.

20. Page 16, Lines 11 – 19: Is the correct interpretation here that Aitken mode particles measured at ENA are continentally derived, while the growth of those particles to CCN size in the MBL is due to biogenic H2SO4? This implies that for ocean ecosystems (at least in the ENA) to have a substantial influence on the MBL CCN population, there must be Aitken mode continental aerosol for the required condensation and growth to occur.

Responses:

Both continental emission and NPF in the FT contribute to the Aitken mode population in FT. However, we cannot quantitively determine the contribution from each of the two sources. Nevertheless, Fig. 9b shows much higher entrained FT At mode particles in spring-summer than entrained CO and BC, suggesting an important contribution of NPF to FT Aitken mode at least during these two seasons. We've added this discussion (see Page 14, Line 37 to Page 15, Line 2):

"Contribution of SSA to the At mode is even smaller than it is to the Ac mode, and is estimated to be no larger than 10 % (Table 4). As a result, the entrainment of FT At mode particles represents the dominant source (Fig. 9a). $\partial_t N_{At|FT}$ is higher in spring-summer while lower in fall-winter, and such seasonal variation is somewhat different from those of CO mixing ratio and EBC mass concentrations (Fig. 9b). These differences may be partially due to stronger new particles formation from biogenic precursors in the FT during spring and summer seasons (Sanchez et al., 2018). The strength of new particle formation is not correlated with CO or EBC concentrations, which are tracers for anthropogenic emissions. The contribution of NPF versus anthropogenic emissions to FT Aitken mode particles cannot be quantitatively determined using data presented here alone, and will be a subject of future study."

Comments by Anonymous Referee #2:

General Comments:

This paper uses two years of observations from the ARM program and a process-based analysis to estimate the factors that are most significant in defining the marine aerosol size distribution at Graciosa Island in the Azores. I find the approach to be systematic and reasonable, the large data set to be valuable and the results to be useful. I have a few little issues with some of the interpretation, but I think this work is worthy of publication in ACP subject to my following comments:

Detailed Comments:

1. The paper reads better at the beginning. The grammar begins to suffer in various places later in the paper. The authors need to carefully read and correct the grammar where needed.

Responses: We've read through the updated manuscript and corrected the grammar carefully.

2. In the abstract and final paragraph (Page 16, lines 11-19), the authors say that the free troposphere (FT) is the major source of CCN to the marine boundary layer (MBL) via direct insertion and insertion of Aitken particles that grow via condensation in the MBL to CCN size; the latter being responsible for about 60% of the CCN in summer. That is a nice result. The authors then say that DMS oxidation is responsible. We cannot deny the likelihood of a contribution from DMS, but we know from work over the past few years that organics may play a significant role in Aitken particle growth. For example, in the Arctic we find growth of Aitken particles in the summer is related to (non-DMS) marine-derived organics at least as much and perhaps more than marine derived sulphate (e.g. papers in the NETCARE special issue of ACP; work done at the Zeppelin Observatory; Willis et al., GRL, 2016; Burkart et al., GRL, 2017; Mungell et al., PNAS, 2017). The Arctic MBL differs from the Pacific and Atlantic MBLs in some respects, but there are similarities and various groups (O'Dowd et al.; Prather et al., etc.) have pointed to (non-DMS related) organics in Aitken particles in the MBL. The authors need to present a slightly more objective summary on this issue. I'm not suggesting to rule out DMS, but don't rule out the possibility of other organic components.

Responses:

We thank the reviewer for raising this point. We agree that while the ENA MBL differs from the Arctic MBL in some respects, it is possible that organics play an important role in the growth of Aitken mode particles. We've added relevant discussions in the updated manuscript. For example, we've added a comment in section 4.2, the condensation part as (see Page 9, Line 32-33):

"Here we assume that H_2SO_4 is the dominant condensate. However, recent studies suggest that organics may play an important role in growth of particles inside MBL, and this is discussed later in section 6.2."

And we've added the discussion into section 6.2 as (see Page 14, Line 14-21):

"Common continental biogenic volatile organic compounds (BVOCs) such as isoprene and monoterpenes typically have very low mixing ratio, and SOA formation from these BVOCs is generally minor in remote marine environment (Kavouras and Stephanou, 2002; Arnold et al., 2009; Gantt et al., 2009; Myriokefalitakis et al., 2010). However, recent studies suggest photochemistry or heterogeneous oxidation

at the sea surface microlayer may represent a substantial source of oxygenated gas-phase organic compounds (OVOCs), which potentially plays an important role in SOA formation and particle growth in the Arctic MBL (Burkart et al., 2017; Willis et al., 2017; Mungall et al., 2017). It is possible that the SOA formation from these OVOCs can contribute to the growth of Aitken mode particles in ENA as well. If so, the contribution to CCN by the growth of Aitken mode particles would be even higher than the estimate here, which is based on condensation of H_2SO_4 only."

3. There is no mention of emissions from ships? What reasons do you have for excluding the possibility of shipping emissions? Related to ships and to the aqueous-phase chemistry and NPF processes, are SO2 concentrations measured at the ARM site? Have you any idea of what they might be? Are they too small to be routinely measured?

Responses:

We thank the reviewer for this point. Data impacted by local ship emissions are screened out and not included in the analyses (SI S1). Langley et al. (2010) show that ship particle emissions, when present, can contribute substantially to particles and CCN. The contribution of the ship particle emissions averaged over large spatial area in remote marine boundary layer remains unclear, and therefore it is not directly treated in this study. As a result, the particles emitted by ships are implicitly grouped into the category of "entrained from the FT".

Several studies (Langley et al., 2010; Corbett and Fischbeck, 1997; Capaldo et al., 1999; Corbett et al., 2007; Wang et al., 2008; Johansson et al., 2017) have shown ship emissions represent a significant source of SO_2 in MBL. In this study, the concentrations of SO_2 and H_2SO_4 are estimated using DMS-SO_2-H_2SO_4 yields based an observation-based parameterization (Russell et al., 1994; Pandis et al., 1994). Therefore, H_2SO_4 formed from ship emitted SO_2, and its contribution to condensational particle growth is implicitly included.

We have clarified this in the revised manuscript. We've added the following in section S1 (Page 2, Line 11-15):

"With this filter, data impacted by local ship emissions are also screened out. Langley et al. (2010) shows that ship particle emissions, when present, can contribute substantially to particle and CCN concentration in the MBL. That condition, if present in ENA, would also be screened out considering the high aerosol number concentration (1000 ~ 3500 cm^{-3}). The contribution of the ship particle emissions averaged over large spatial area in remote marine boundary layer remains unclear, therefore it is not directly treated in this study."

With regards to regional ship emissions, we've added relevant discussions in section 6.2 as (see Page 14, Line 22-26):

"Several studies (Langley et al., 2010; Corbett and Fischbeck, 1997; Capaldo et al., 1999; Corbett et al., 2007; Wang et al., 2008; Johansson et al., 2017) have shown that ship emissions represent a significant source of SO_2 in MBL. In this study, the concentrations of SO_2 and H_2SO_4 are estimated using DMS-SO_2-H_2SO_4 yields based an observation-based parameterization (Russell et al., 1994; Pandis et al., 1994).

Therefore, H_2SO_4 formed from ship emitted SO_2, and its contribution to condensational particle growth is implicitly included."

Unfortunately, SO_2 measurement is not available at the ENA site. Here we assume NPF is rare inside MBL, and estimated SO_2 concentration is used to qualitatively demonstrate that the aqueous-phase chemistry has negligible influence on the particle number concentration of each mode (see responses to comment #16).

4. Abstract, lines 20-21 – Define the size ranges for At, Ac and LA modes here.

Responses: The information has been added as (see Page 1, Line 23-24):

"Submicron aerosol size distribution typically consists of three modes: Aitken (At, diameter D_p < ~100 nm), Accumulation (Ac, D_p within ~100 to ~300 nm), and Larger Accumulation (LA, D_p > ~300 nm) modes,…".

5. Abstract, line 28 – How is "the estimate based on major sources and sinks" made?

Responses: We've changed the expression into "generally agrees with the steady-state concentration estimated from major sources and sink."

6. Page 2, line 20 – For previous aerosol studies, consider Phinney et al., Deep Sea Research (2006) and Langley et al. ACP (2010).

Responses: The references have been added as suggested.

7. Page 2, lines 23-24 – "cloud coalescence scavenging" or "coalescence scavenging in cloud" or something with cloud factored in.

Responses: The expression has been changed into "in-cloud coalescence scavenging" throughout as suggested.

8. Page 2, line 39 – Consider Leaitch et al., ACP (2010) that looks at two cases of aerosols and MBL clouds over the Western Atlantic. Also, they found the supersaturations to be between 0.1 and 0.2% depending on the aerosol concentrations.

Responses:

This paragraph focused on campaigns in Eastern North Atlantic only. We referred to the Leaitch et al., ACP (2010) paper in discussions of typical supersaturation levels for marine low clouds instead (Page 9, Line1-2):

"The maximum supersaturation near the cloud base where *CCN* activation occurs is typically 0.2 % for marine low clouds (Wood et al., 2012; Clarke and Kapustin, 2010; Leaitch et al., 2010)."

9. Page 3, lines 26-27 – Indicate how the inlet has been evaluated for transmission losses of the larger particles (i.e. 5-10 um diameter).

Responses:

The transmission losses for the 5-10 um size range are not corrected. However, as we only examine the relative trends of the coarse mode optical properties and their correlations with other aerosol properties, we do not expect this will affect the results or conclusions from this study.

We've clarified this by including following description in the revised manuscript (see Page 3, Line 35 to 37):

"Potential particle losses for large particles (i.e., in the diameter range of 5 ~10 μm) are not corrected. However, we do not expect the losses affect the relative trends of PM_c B_{sca} presented here (section 5), or the correlation among PM_c B_{sca} and V_{LA} (Fig. 6c)."

10. Section 2.2.2 – Presumably, cloud base height and cloud thickness are used in the analysis, but at this point (Section 2.2.2) it is unclear why cloud properties are discussed. Maybe on page 3 (around lines 5-6) or at the beginning of 2.2.2?

Responses:

We've added a paragraph at the beginning of section 2.2.2 as (see Page 4, Line 3-4):

"The cloud and MBL properties are needed to estimate some of the key controlling processes that drives aerosol properties (see section 4 for more details). Key parameter needed included the MBL height, cloud thickness and cloud fraction."

11. Page 5, line 23 – due to changes in tropopause height.

Responses:

The expression has been modified into (see Page 5, Line 27-28):

"In contrast, CO and O_3 in ENA show a summer minimum and spring-winter maximum, which is consistent with the FT entrainment as the dominant source and corresponding seasonal variations in tropopause height. This suggests minor contributions from local emissions and in-situ photochemistry (Parrish et al., 1998; Fischer et al., 2003; Mao and Talbot, 2004)."

12. Your BC is measured from estimated absorption based on a filter transmission technique. The standard reference to this is Equivalent Back Carbon or EBC (Petzold et al., 2013) rather than BC. You should adopt that nomenclature.

Responses:

The expression has been changed throughout as suggested, with a notion added in section 2 as (see Page 6, Lines 2-3):

"After these episodes are excluded, the equivalent black carbon (EBC, following the naming convection suggested by Petzold et al. (2013)) mass concentrations were estimated from PM_1 B_{abs} with an assumed mass absorbing cross section of 7.5 m^2 g^{-1} at 529 nm (Bond et al., 2013)."

13. Page 6, line 2 - define "Pcb"

Responses: The definition (precipitation rate at cloud base) has been added as suggested.

14. Page 6, line 35 - Particles "activate" and droplets "nucleate".

Responses: The word "activated" has been deleted.

15. Page 7, line 3 – Dry deposition may be slower on average, but you are discussing processes that happen over a week to 10 days. Please discuss further.

Responses:

In previous work comparing the contribution of dry and wet depositions (Henzing et al., 2006; Wood et al., 2012; Mohrmann et al., 2018), the time discontinuity in wet depositions are already considered, as also did in our study by taking into account the cloud fraction. The results show that for submicron MBL aerosols, the contribution of dry deposition is very small, with a fractional contribution generally < 5% in total (dry and wet) removal processes (Henzing et al., 2006), and absolute loss rates "unlikely to exceed 2 cm^{-3} d^{-1}" (Wood et al., 2012) under most circumstances.

This point is further clarified in the manuscript as (see Page 7, Line 11-14):

"In addition, dry deposition is usually much slower compared to wet deposition for submicron particles, even after considering in the in-cloud possibility, f_{cloud}, which reflects the time and spatial discontinuity of the wet deposition processes (see the in-cloud scavenging part in section 4.2) (Lewis and Schwartz, 2004; Henzing et al., 2006; Wood et al., 2012; Mohrmann et al., 2018). Thus, it is neglected in further analysis."

16. Page 8, lines 32-34 - Using a limit of 100 nm diameter for the Ac particles, you eliminate the potential for some larger Aitken particles to grow into the Ac mode via S(IV) oxidation. Without relatively large amounts of SO2, it will be very difficult for the Ac particles to grow into the LA mode. While still a big ask, for relatively low SO2, as seems more likely in the MBL you have constrained, the probability of growing 80 nm particles to 120 nm is more likely. What precursor concentrations do you use for your analysis?

Responses:

There may be some misunderstanding here. In this section we're discussing the aqueous-phase reactions inside cloud droplets. As has been clearly outlined in section 4 and depicted in Fig. 5, Aitken mode particles are not CCN and thus are not considered in aqueous-phase reactions. That is due to the much higher liquid water content and thus much higher aqueous-phase reaction rates in cloud droplets than in interstitial aerosols. In-cloud sulfate production can contribute to the growth of the Aitken mode aerosols, but that only occurs after the Aitken mode particles have already grown to *CCN* (i.e. into Ac mode size ranges)

through condensation. We've added a paragraph at the start of this section to further clarify this (Page 9, Line 9-14):

"The aqueous-phase reaction (i.e., in-cloud production of sulfate) rate is positively related the liquid water content (Seinfeld and Pandis, 2016; Meng and Seinfeld, 1994; Pandis et al., 1990; Cheng et al., 2016). As the liquid water content of cloud droplets are orders-of-magnitude higher than that of interstitial aerosols, only aqueous-phase reactions inside the cloud droplets are considered here (Pandis et al., 1990). As a result, the aqueous-phase reactions only promote the growth of *CCN* (i.e., Ac and LA mode particles), the influence of aqueous phase reactions on the Aitken mode particles is neglected until they grow to *CCN* sizes through condensation (Hoppel et al., 1994; Pandis et al., 1990)."

The precursor concentrations are given in section 4.2, the condensation part. It was described as (see Page 9, Line 27-30):

(The annual mean H_2SO_4) "is assumed to be 1.0 ppt (Pandis et al., 1994), while being 1.4, 1.3, 1.1 and 0.2 ppt in spring, summer, fall and winter, respectively. This seasonal variation in v_i is based on the monthly dimethyl sulfide (DMS) fluxes (assumed to be 7.0, 5.4, 2.9 and 1.0 μmol m^{-2} day^{-1} in spring, summer, fall and winter, respectively) given in previous studies in the North Atlantic Ocean (Tarrasón et al., 1995), and the proposed dependence of H_2SO_4 on DMS flux at the observed fluxes ranges (Pandis et al., 1994; Russell et al., 1994)."

17. Page 11, line 8-9 – Is the strong correlation between N(LA) and WS a result of using equation 2?

Responses: Not likely. The N_{LA} is from fitting of the observation data, not calculated by Eq. 2.

18. Page 11, line 19 – "Given the large sizes of LA particles and that we have excluded dust, we do not: : :"

Responses: The expression has been corrected as suggested.

19. Page 11, line 21 – ": : :the concentration of LA particles from the FT is negligible: : :"

Responses: The expression has been corrected as suggested.

20. Page 12, line 7 – The decreasing At with increasing WS could indicate some wind associated dilution of oceanic sources of At particles.

Responses:

The MBL height likely play a more important role in the dilution of MBL aerosol than WS. A more plausible explanation may be that, the higher N_{LA} at higher WS will increase the coagulation sink of Aitken mode aerosols. As coagulation is the dominant sink for Aitken mode aerosols, this can better explain the negative correlation of N_{At} with WS.

We have added this potential explanation to the manuscript as (see Page 12, Line 7-9):

"Unlike N_{LA}, N_{Ac} is independent of the WS, and N_{At} decreases with increasing WS (Fig. 7), indicating relatively minor contributions from SSA to At and Ac modes. The negative correlation between N_{At} and WS may be due to the enhanced N_{LA} with increasing WS (Fig. 6), and thus enhanced coagulation loss for Aitken mode particles (see section 4.2 and section 6.3)."

21. Page 14, lines 25-26 - That does not mean there is no contribution from anthropogenic emissions. It could be a case of the contribution being high in spring and low in summer.

Responses:

We have further clarified this in the revised manuscript (see Page 14, Line 38 to Page 15, Line 2):

"$\partial_t N_{At|FT}$ is higher in spring-summer while lower in fall-winter, and such seasonal variation is somewhat different from those of CO mixing ratio and EBC mass concentrations (Fig. 9b). These differences may be partially due to stronger new particles formation from biogenic precursors in the FT during spring and summer seasons (Sanchez et al., 2018). The strength of new particle formation is not correlated with CO or EBC concentrations, which are tracers for anthropogenic emissions. The contribution of NPF versus anthropogenic emissions in FT Aitken mode particles, cannot be quantitively determined using data presented here alone, and will be a subject of future study."

22. Page 15, line 19 – It is 70 nm in the figures, not 60nm. I assume 70 nm is correct due to the noise issues that appear to be common in the first one or two channels of the UHSAS.

Responses: The expression has been corrected to 70 nm throughout as suggested, and we added a notion below Table 1 as:

"[a] In fact the lower size limit of UHSAS is 60 nm. Here we used only data larger than 70 nm to avoid noises sometimes observed in the first several channels of the UHSAS."

23. Page 15, line 24 – Sources of LA particles are dominated by SSA.

Responses: The expression has been corrected as suggested.

24. Page 15, line 24 – "dilution by entrained FT air". In order to dilute the LA particles with FT air, presumably some of the LA particles must enter the FT. Could that be an important FT source somewhere downwind?

Responses:

We don't think so. The entrainment process is not an exchange between FT and MBL. Instead, FT air is entrained into and stays inside the MBL (Stull, 2012). The entrainment counteracts the large-scale substance in ENA, and help sustain the MBL height (Stull, 2012; Mohrmann et al., 2018; Wood and Bretherton, 2004). While we agree that some LA particles may enter the FT through deeper convection, it is worth noting that these convections are often associated with precipitation that efficiently removes LA mode particles. Therefore the influence of such process on FT particle population is likely negligible.

25. Page 16, lines 14-15 – Can marine emissions be a factor here also, if they are lofted above the MBL somewhere and return to the MBL somewhere else?

Responses: Please refer to our response to comment #24.

References

Arnold, S. R., Spracklen, D. V., Williams, J., Yassaa, N., Sciare, J., Bonsang, B., Gros, V., Peeken, I., Lewis, A. C., Alvain, S., and Moulin, C.: Evaluation of the global oceanic isoprene source and its impacts on marine organic carbon aerosol, Atmos. Chem. Phys., 9, 1253-1262, 10.5194/acp-9-1253-2009, 2009.

Bond, T. C., Doherty, S. J., Fahey, D. W., Forster, P. M., Berntsen, T., DeAngelo, B. J., Flanner, M. G., Ghan, S., Kärcher, B., Koch, D., Kinne, S., Kondo, Y., Quinn, P. K., Sarofim, M. C., Schultz, M. G., Schulz, M., Venkataraman, C., Zhang, H., Zhang, S., Bellouin, N., Guttikunda, S. K., Hopke, P. K., Jacobson, M. Z., Kaiser, J. W., Klimont, Z., Lohmann, U., Schwarz, J. P., Shindell, D., Storelvmo, T., Warren, S. G., and Zender, C. S.: Bounding the role of black carbon in the climate system: A scientific assessment, Journal of Geophysical Research: Atmospheres, 118, 5380-5552, 10.1002/jgrd.50171, 2013.

Burkart, J., Hodshire, A. L., Mungall, E. L., Pierce, J. R., Collins, D. B., Ladino, L. A., Lee, A. K. Y., Irish, V., Wentzell, J. J. B., Liggio, J., Papakyriakou, T., Murphy, J., and Abbatt, J.: Organic Condensation and Particle Growth to CCN Sizes in the Summertime Marine Arctic Is Driven by Materials More Semivolatile Than at Continental Sites, Geophysical Research Letters, 44, 10,725-710,734, doi:10.1002/2017GL075671, 2017.

Campuzano-Jost, P., Clark, C. D., Maring, H., Covert, D. S., Howell, S., Kapustin, V., Clarke, K. A., Saltzman, E. S., and Hynes, A. J.: Near-Real-Time Measurement of Sea-Salt Aerosol during the SEAS Campaign: Comparison of Emission-Based Sodium Detection with an Aerosol Volatility Technique, Journal of Atmospheric and Oceanic Technology, 20, 1421-1430, 10.1175/1520-0426(2003)020<1421:nmosad>2.0.co;2, 2003.

Capaldo, K., Corbett, J. J., Kasibhatla, P., Fischbeck, P., and Pandis, S. N.: Effects of ship emissions on sulphur cycling and radiative climate forcing over the ocean, Nature, 400, 743, 10.1038/23438, 1999.

Cheng, Y., Zheng, G., Wei, C., Mu, Q., Zheng, B., Wang, Z., Gao, M., Zhang, Q., He, K., Carmichael, G., Pöschl, U., and Su, H.: Reactive nitrogen chemistry in aerosol water as a source of sulfate during haze events in China, Science Advances, 2, 10.1126/sciadv.1601530, 2016.

Clarke, A., and Kapustin, V.: Hemispheric Aerosol Vertical Profiles: Anthropogenic Impacts on Optical Depth and Cloud Nuclei, Science, 329, 1488-1492, 10.1126/science.1188838, 2010.

Corbett, J. J., and Fischbeck, P.: Emissions from Ships, Science, 278, 823-824, 10.1126/science.278.5339.823, 1997.

Corbett, J. J., Winebrake, J. J., Green, E. H., Kasibhatla, P., Eyring, V., and Lauer, A.: Mortality from Ship Emissions: A Global Assessment, Environmental Science & Technology, 41, 8512-8518, 10.1021/es071686z, 2007.

Gantt, B., Meskhidze, N., and Kamykowski, D.: A new physically-based quantification of marine isoprene and primary organic aerosol emissions, Atmos. Chem. Phys., 9, 4915-4927, 10.5194/acp-9-4915-2009, 2009.

Henzing, J. S., Olivié, D. J. L., and van Velthoven, P. F. J.: A parameterization of size resolved below cloud scavenging of aerosols by rain, Atmos. Chem. Phys., 6, 3363-3375, 10.5194/acp-6-3363-2006, 2006.

Hoppel, W. A., Frick, G. M., Fitzgerald, J. W., and Larson, R. E.: Marine boundary layer measurements of new particle formation and the effects nonprecipitating clouds have on aerosol size distribution, Journal of Geophysical Research: Atmospheres, 99, 14443-14459, 10.1029/94JD00797, 1994.

Johansson, L., Jalkanen, J.-P., and Kukkonen, J.: Global assessment of shipping emissions in 2015 on a high spatial and temporal resolution, Atmospheric Environment, 167, 403-415, https://doi.org/10.1016/j.atmosenv.2017.08.042, 2017.

Kavouras, I. G., and Stephanou, E. G.: Particle size distribution of organic primary and secondary aerosol constituents in urban, background marine, and forest atmosphere, Journal of Geophysical Research: Atmospheres, 107, AAC 7-1-AAC 7-12, doi:10.1029/2000JD000278, 2002.

Kettle, A. J., Andreae, M. O., Amouroux, D., Andreae, T. W., Bates, T. S., Berresheim, H., Bingemer, H., Boniforti, R., Curran, M. A. J., DiTullio, G. R., Helas, G., Jones, G. B., Keller, M. D., Kiene, R. P., Leck, C., Levasseur, M., Malin, G., Maspero, M., Matrai, P., McTaggart, A. R., Mihalopoulos, N., Nguyen, B. C., Novo, A., Putaud, J. P., Rapsomanikis, S., Roberts, G., Schebeske, G., Sharma, S., Simó, R., Staubes, R., Turner, S., and Uher, G.: A global database of sea surface dimethylsulfide (DMS) measurements and a procedure to predict sea surface DMS as a function of latitude, longitude, and month, Global Biogeochemical Cycles, 13, 399-444, 10.1029/1999GB900004, 1999.

Langley, L., Leaitch, W. R., Lohmann, U., Shantz, N. C., and Worsnop, D. R.: Contributions from DMS and ship emissions to CCN observed over the summertime North Pacific, Atmos. Chem. Phys., 10, 1287-1314, 10.5194/acp-10-1287-2010, 2010.

Leaitch, W. R., Lohmann, U., Russell, L. M., Garrett, T., Shantz, N. C., Toom-Sauntry, D., Strapp, J. W., Hayden, K. L., Marshall, J., Wolde, M., Worsnop, D. R., and Jayne, J. T.: Cloud albedo increase from carbonaceous aerosol, Atmos. Chem. Phys., 10, 7669-7684, 10.5194/acp-10-7669-2010, 2010.

Lewis, E. R., and Schwartz, S. E.: Sea salt aerosol production: mechanisms, methods, measurements, and models-A critical review, American geophysical union, 2004.

Meng, Z., and Seinfeld, J. H.: On the Source of the Submicrometer Droplet Mode of Urban and Regional Aerosols, Aerosol Science and Technology, 20, 253-265, 10.1080/02786829408959681, 1994.

Mohrmann, J., Wood, R., McGibbon, J., Eastman, R., and Luke, E.: Drivers of Seasonal Variability in Marine Boundary Layer Aerosol Number Concentration Investigated Using a Steady State Approach, Journal of Geophysical Research: Atmospheres, 123, 1097-1112, 10.1002/2017JD027443, 2018.

Mungall, E. L., Abbatt, J. P. D., Wentzell, J. J. B., Lee, A. K. Y., Thomas, J. L., Blais, M., Gosselin, M., Miller, L. A., Papakyriakou, T., Willis, M. D., and Liggio, J.: Microlayer source of oxygenated volatile organic compounds in the summertime marine Arctic boundary layer, Proceedings of the National Academy of Sciences, 114, 6203-6208, 10.1073/pnas.1620571114, 2017.

Myriokefalitakis, S., Vignati, E., Tsigaridis, K., Papadimas, C., Sciare, J., Mihalopoulos, N., Facchini, M. C., Rinaldi, M., Dentener, F. J., Ceburnis, D., Hatzianastasiou, N., O'Dowd, C. D., van Weele, M., and Kanakidou, M.: Global Modeling of the Oceanic Source of Organic Aerosols, Advances in Meteorology, 2010, 16, 10.1155/2010/939171, 2010.

Pandis, S. N., Seinfeld, J. H., and Pilinis, C.: Chemical composition differences in fog and cloud droplets of different sizes, Atmospheric Environment. Part A. General Topics, 24, 1957-1969, https://doi.org/10.1016/0960-1686(90)90529-V, 1990.

Pandis, S. N., Russell, L. M., and Seinfeld, J. H.: The relationship between DMS flux and CCN concentration in remote marine regions, Journal of Geophysical Research: Atmospheres, 99, 16945-16957, 10.1029/94JD01119, 1994.

Petzold, A., Ogren, J. A., Fiebig, M., Laj, P., Li, S. M., Baltensperger, U., Holzer-Popp, T., Kinne, S., Pappalardo, G., Sugimoto, N., Wehrli, C., Wiedensohler, A., and Zhang, X. Y.: Recommendations for reporting "black carbon" measurements, Atmos. Chem. Phys., 13, 8365-8379, 10.5194/acp-13-8365-2013, 2013.

Quinn, P. K., Coffman, D. J., Johnson, J. E., Upchurch, L. M., and Bates, T. S.: Small fraction of marine cloud condensation nuclei made up of sea spray aerosol, Nature Geosci, advance online publication, 10.1038/ngeo3003 http://www.nature.com/ngeo/journal/vaop/ncurrent/abs/ngeo3003.html#supplementary-information, 2017.

Russell, L. M., Pandis, S. N., and Seinfeld, J. H.: Aerosol production and growth in the marine boundary layer, Journal of Geophysical Research: Atmospheres, 99, 20989-21003, doi:10.1029/94JD01932, 1994.

Sanchez, K. J., Chen, C.-L., Russell, L. M., Betha, R., Liu, J., Price, D. J., Massoli, P., Ziemba, L. D., Crosbie, E. C., Moore, R. H., Müller, M., Schiller, S. A., Wisthaler, A., Lee, A. K. Y., Quinn, P. K., Bates, T. S., Porter, J., Bell, T. G., Saltzman, E. S., Vaillancourt, R. D., and Behrenfeld, M. J.: Substantial Seasonal Contribution of Observed Biogenic Sulfate Particles to Cloud Condensation Nuclei, Scientific Reports, 8, 3235, 10.1038/s41598-018-21590-9, 2018.

Seinfeld, J. H., and Pandis, S. N.: Atmospheric chemistry and physics: from air pollution to climate change, John Wiley & Sons, 2016.

Stull, R. B.: An introduction to boundary layer meteorology, Springer Science & Business Media, 2012.

Tarrasón, L., Turner, S., and Fløisand, I.: Estimation of seasonal dimethyl sulphide fluxes over the North Atlantic Ocean and their contribution to European pollution levels, Journal of Geophysical Research: Atmospheres, 100, 11623-11639, 10.1029/95JD00849, 1995.

Wang, C., Corbett, J. J., and Firestone, J.: Improving Spatial Representation of Global Ship Emissions Inventories, Environmental Science & Technology, 42, 193-199, 10.1021/es0700799, 2008.

Willis, M. D., Köllner, F., Burkart, J., Bozem, H., Thomas, J. L., Schneider, J., Aliabadi, A. A., Hoor, P. M., Schulz, H., Herber, A. B., Leaitch, W. R., and Abbatt, J. P. D.: Evidence for marine biogenic influence on summertime Arctic aerosol, Geophysical Research Letters, 44, 6460-6470, doi:10.1002/2017GL073359, 2017.

Wood, R., and Bretherton, C. S.: Boundary Layer Depth, Entrainment, and Decoupling in the Cloud-Capped Subtropical and Tropical Marine Boundary Layer, Journal of Climate, 17, 3576-3588, 10.1175/1520-0442(2004)017<3576:bldead>2.0.co;2, 2004.

Wood, R., Leon, D., Lebsock, M., Snider, J., and Clarke, A. D.: Precipitation driving of droplet concentration variability in marine low clouds, Journal of Geophysical Research: Atmospheres, 117, n/a-n/a, 10.1029/2012JD018305, 2012.

Marine boundary layer aerosol in Eastern North Atlantic: seasonal variations and key controlling processes

Guangjie Zheng[1,2], Yang Wang[1,2], Allison C. Aiken[3], Francesca Gallo[3], Michael P. Jensen[1], Pavlos Kollias[4], Chongai Kuang[1], Edward Luke[1], Stephen Springston[1], Janek Uin[1], Robert Wood[5], and Jian Wang[1,2,*]

[1] Environmental and Climate Science Department, Brookhaven National Laboratory, Upton, New York, USA
[2] Center for Aerosol Science and Engineering, Department of Energy, Environmental and Chemical Engineering, Washington University in St. Louis, Missouri, USA
[3] Earth System Observations, Los Alamos National Laboratory, Los Alamos, New Mexico, USA
[4] School of Marine and Atmospheric Sciences, Stony Brook University, State University of New York, Stony Brook, New York, USA
[5] Department of Atmospheric Science, University of Washington, Seattle, USA

Correspondence to: J. Wang (jian@wustl.edu)

Abstract

The response of marine low cloud systems to changes in aerosol concentration represents one of the largest uncertainties in climate simulations. Major contributions to this uncertainty derive from poor understanding of aerosol under natural conditions and the perturbation by anthropogenic emissions. The Eastern North Atlantic (ENA) is a region of persistent but diverse marine boundary layer (MBL) clouds, whose albedo and precipitation are highly susceptible to perturbations in aerosol properties. In this study, we examine MBL aerosol properties, trace gas mixing ratios, and meteorological parameters measured at the Atmospheric Radiation Measurement Climate Research Facility's ENA site on Graciosa Island, Azores, Portugal, during a three-year period from 2015 to 2017. Measurements impacted by local pollutions on Graciosa Island and during occasional intense biomass burning and dust events are excluded from this study. Submicron aerosol size distribution typically consists of three modes: Aitken (At, diameter D_p < ~100 nm), Accumulation (Ac, D_p within ~100 to ~300 nm), and Larger Accumulation (LA, D_p > ~300 nm) modes, with average number concentrations (denoted as N_{At}, N_{Ac} and N_{LA} below) of 330, 114, and 14 cm^{-3}, respectively. N_{At}, N_{Ac} and N_{LA} show contrasting seasonal variations, suggesting different sources and removal processes. N_{LA} is dominated by sea spray aerosol (SSA), and is higher in winter and lower in summer. This is due to the seasonal variations of SSA production, in-cloud coalescence scavenging, and dilution by entrained free troposphere (FT) air. In comparison, SSA typically contributes a relatively minor fraction to N_{At} (10 %) and N_{Ac} (21 %) on an annual basis. In addition to SSA, sources of Ac mode particles include entrained of FT aerosols and condensation growth of Aitken mode particles inside MBL, while in-cloud coalescence scavenging is the major sink of N_{Ac}. The observed seasonal variation of N_{Ac}, being higher in summer and lower in winter, generally agrees with the steady-state concentration estimated from major sources and sinks. N_{At} is mainly controlled by entrainment of FT aerosol, coagulation loss, and growth of Aitken mode particles into the Ac mode size range. Our calculation suggests that besides the direct contribution from entrained FT Ac mode particles, growth of entrained FT Aitken mode particles in the MBL also represent a substantial source of cloud condensation nuclei (*CCN*), with the highest contribution potentially reaching 60 % during summer. The growth of Aitken mode particles to *CCN* size is an expected result of the condensation of sulfuric acid, a product from dimethyl sulfide oxidation, suggesting that ocean ecosystems may have a substantial influence on MBL *CCN* populations in ENA.

1 Introduction

Low clouds, especially stratocumulus, are the dominant cloud type in terms of spatial coverage of the Earth's surface, and are of vital importance to the Earth's climate (Wood, 2012). Major climate effects of low clouds derive from their reflection of solar radiation (Seinfeld and Pandis, 2016). The key parameters for quantifying climate effects of low clouds are the albedo (i.e., cloud reflectivity) and the cloud coverage, both of which are particularly sensitive to perturbations of aerosols. The concentration of cloud condensation nuclei (*CCN*) strongly influences the number concentration and sizes of cloud droplets and therefore the effective albedo of low clouds (i.e., first indirect effect of aerosol) (Twomey, 1974; Seinfeld and Pandis, 2016; Dong et al., 2015), especially in clean environments such as the remote marine boundary layer (MBL) (Reutter et al., 2009). In addition, *CCN* concentration and aerosol size distribution also influence cloud amount by impacting drizzle formation and precipitation (i.e., second indirect effect of aerosol) (Albrecht, 1989; Liu and Daum, 2004; Liu et al., 2006; Wood, 2005; Rémillard et al., 2012; Dong et al., 2014).

Currently, the aerosol indirect effects of marine low cloud systems remain one of the major uncertainties in climate change simulations (Lohmann and Feichter, 2005; Bony and Dufresne, 2005; Bony et al., 2006; Wood, 2012). This large uncertainty is to a large degree a result of the incomplete understanding and therefore representations of aerosol properties, and the response of marine low clouds to aerosol changes. Therefore, it is imperative to understand MBL aerosol properties under natural conditions, the perturbation due to anthropogenic emissions, and the underlying controlling processes. The properties of aerosols in the remote MBL can be influenced by a variety of processes, including entrainment from the free troposphere (FT), production of sea spray aerosol (SSA), processing of aerosol particles both inside clouds and in clear air, depositions, and horizontal advection (Quinn and Bates, 2011; Wood et al., 2012). Previous studies (O'Dowd et al., 2004; Clarke et al., 2013; Quinn et al., 2017; Wood et al., 2017; Pierce et al., 2015; Prather et al., 2013; Russell et al., 2010; Sanchez et al., 2018; Phinney et al., 2006; Langley et al., 2010) have greatly advanced our understanding of MBL aerosols, especially in the relative contributions of SSA versus long-range transported pollution in terms of the *CCN* budget (Blot et al., 2013; Clarke and Kapustin, 2010; Clarke et al., 2013; Quinn et al., 2017), and the removal of *CCN* by in-cloud coalescence scavenging (Wood et al., 2012). However, we are still lacking a quantitative understanding of the controlling processes sufficient to serve as a reliable foundation for developing global climate model parameterizations and representations that will adequately simulate aerosol in past, current, and future climates. The relative importance, the influence on different particle size ranges, and spatiotemporal variations of these processes are still not well quantified.

The Eastern North Atlantic (ENA) is a region of persistent but diverse subtropical MBL clouds (Wood et al., 2015). Aerosols arriving in the ENA are of diverse origins, varying from marine clean air masses to air masses that are strongly influenced by continental emissions from North America or northern Europe (O'Dowd and Smith, 1993; Wood et al., 2015). As a result, ENA is among the regions with strong but uncertain aerosol indirect forcing (Carslaw et al., 2013). Several field campaigns, including the North Atlantic Regional Experiment (NARE) campaign during 1991 to 2001 (Parrish et al., 1998), the Atlantic Stratocumulus Transition Experiment (ASTEX) during June 1992, the 2nd Aerosol Characterization Experiment (ACE-2) during summer 1997, and the Clouds, Aerosol, and Precipitation in the Marine Boundary Layer (CAP-MBL) campaign (Wood et al., 2015) from May 2009 to December 2010 took place in ENA. However, they are either more focused on other subjects (e.g., ozone chemistry for NARE (Parrish et al., 1998) and cloud properties for CAP-MBL (Wood et al., 2015), or are short-term studies (e.g., ACE-2 (Raes et al., 2000), ASTEX (Albrecht et al., 1995)). To our knowledge, the variation of aerosol properties and their controlling processes have not been systematically studied using long term observation in the ENA.

Recently, a permanent ENA site was established by the Department of Energy Atmospheric Radiation Measurement (ARM) (Mather and Voyles, 2013) Climate Research Facility on Graciosa Island in the Azores, Portugal, providing an invaluable opportunity to study MBL aerosol properties and their interactions with low clouds. In this study, we examine the long-term variation of aerosol properties, trace gas mixing ratios, and meteorological parameters measured at the ARM ENA site from 2015 to 2017 (section 2). The characteristics of the aerosol properties and their seasonal variations are summarized (section 3). The governing equations of number concentration are established for different modes of MBL aerosol at the ENA site (section 4). Subsequently, the seasonal variations of aerosol properties for different particle size modes are explained using key processes identified (section 5 and 6). Finally, we present an overall picture of the processes that drive MBL aerosol properties in ENA, and the implications are discussed (section 7).

2 Measurement

2.1 Measurement overview

Measurements of trace gases, meteorological parameters, aerosol and cloud properties are conducted at the ENA site, located on Graciosa Island in the Azores, Portugal (39° 5' 30" N, 28° 1' 32" W, 30.48 m above mean sea level). The ENA site was initially set up in late 2013, with additional measurements added subsequently. The primary measurements used in this study and the available time periods are listed in Table 1. The measurements of trace gases (e.g., CO) and aerosol properties were first screened for impact from local pollution sources (see Supporting Information (SI) section S1). All measurements are then averaged into 1-hour intervals. Here we use three-years of data from Jan. 2015 to Dec. 2017 to show the long-term variations and correlations among different parameters. For evaluation of the contributions of different controlling processes (section 4), one-year of data from Sept. 2016 to Aug. 2017 are used, during which period most of the measurements are available.

2.2 Data corrections and derivations

2.2.1 Optical properties

Aerosol absorbing (B_{abs}) and scattering (B_{sca}) coefficients are measured by a three-wavelength PSAP and a Nephelometer, respectively (Table 1). These two instruments share a common inlet, and the 50 % cut size of the inlet switches between 1 and 10 μm every hour (Springston, 2016). The corresponding B_{sca} and B_{abs} are denoted by "PM_1" and "PM_{10}", respectively. In addition, properties of coarse mode ($1 < D_p < 10$ μm) aerosols, PM_c, were derived by the difference between PM_{10} and PM_1. For example, "PM_c B_{sca}" refers to the difference between PM_{10} B_{sca} and PM_1 B_{sca} hereafter, and PM_c B_{abs} is defined similarly.

The mass flow calibration and filter loading correction are already applied to the PASP data in the ARM data archive (Springston, 2016). In this study, additional corrections of contribution due to scattering for B_{abs} (Bond et al., 1999; Virkkula et al., 2005; Virkkula, 2010; Costabile et al., 2013), and truncation and angular illumination for B_{sca} (Anderson and Ogren, 1998; Müller et al., 2011) are applied, and the procedure is detailed in SI section S2. The corrected PM_1 B_{sca} shows strong correlation (correlation coefficient being 0.84) with the volume of PM_1 derived from UHSAS size distribution (Fig. S2). Potential particle losses for large particles (i.e., in the diameter range of 5 ~10 μm) are not corrected. However, we do not expect the losses affect the relative trends of PM_c B_{sca} presented here (section 5), or the correlation among PM_c B_{sca} and V_{LA} (Fig. 6c).

2.2.2 Cloud and MBL properties

Properties of cloud and MBL, including MBL height, cloud thickness and cloud fraction are needed to estimate some of the key controlling processes that drive aerosol properties (see section 4 for more details). The MBL height, H_{MBL}, is derived from the backscatter signal from the Ceilometer CL31 (Morris, 2012). Briefly, it is determined from the gradient of an idealized backscatter profile, the parameters of which are derived from fitting of the observed profile (Eresmaa et al., 2006). As the first boundary layer height given in the ceilometer data product is usually the surface layer (Lewis and Schwartz, 2004) below 100 m (Münkel et al., 2007; Emeis et al., 2007; Emeis et al., 2008; Haeffelin et al., 2012; Morris, 2012), H_{MBL} is chosen as the highest boundary layer height below 3 km (Zhou et al., 2015; Rémillard and Tselioudis, 2015; Rémillard et al., 2012).

Cloud thickness h is derived by combining H_{MBL} and the cloud base height derived from ceilometer data. In ENA, H_{MBL} usually represents the top height of boundary layer clouds (Rémillard et al., 2012). When multiple layers of clouds are detected, the layers with cloud-base heights higher than H_{MBL} are first excluded, after which the highest layer is chosen to exclude potential influence of near-ground thin clouds. The cloud thickness h is then defined as the difference between H_{MBL} (cloud top) and the base height of the chosen cloud. The value of h derived using the above approach is in general agreement with previous observations (Rémillard et al., 2012).

The cloud fraction, p_{cloud}, is determined by the detection status information from the ceilometer (Morris, 2012). It is equal to the fraction of time with a detected boundary layer cloud base, or a determined full obscuration. Precipitation rate at cloud base is retrieved from the vertically pointing K-band cloud radar (Atmospheric Radiation Measurement Climate Research Facility, 1990) and the ceilometer (Morris, 2012) following the method of O'Connor et al. (2005).

3. Seasonal variation in synoptic conditions, trace gas mixing ratios, and aerosol properties in ENA

3.1 Air mass origin

One major source of MBL aerosol in ENA is the entrainment of FT air, which contains both particles from long-range transport of continental pollutions and those formed through new particle formation (NPF) in the FT (Quinn and Bates, 2011; Sanchez et al., 2018). To examine the contribution from continental emissions and its seasonal variation, we analyze the back trajectories of air masses arriving at the ENA site. The cluster analysis results of 4 representative months from Sept. 2016 to Aug. 2017 (i.e., the main study period, see section 2.1) are shown in Fig. 1. Results from other periods from 2015 to 2017 are similar (not shown).

Most of the air masses arriving at the ENA site can be classified as one of the four clusters originating from North America, northern Europe, the Arctic, and the recirculating flow around the Azores high, respectively (O'Dowd and Smith, 1993; Wood et al., 2015). Among these clusters, the Azores high air masses usually linger within the MBL, as indicated by their stable and low-level trajectories (e.g., blue and red trajectory clusters in Fig. 1b). In comparison, other air masses usually undergo long-range transport within the FT before descending into MBL. In addition, some air masses originating in the continental boundary layer were lofted up, and then subsided into the MBL within 10 days (e.g., blue trajectory cluster in Fig. 1c).

The percentage of occurrence for each cluster shows strong seasonal variations (Fig. 1, Fig. S3). During fall (Fig. 1c, Fig. S3c) and winter (Fig. 1d, Fig. S3d), air masses influenced by anthropogenic emissions from North American (red lines) dominate, with the influence of clean maritime flow and northern European flow. In spring (Fig. 1a, Fig. S3a), contributions from Arctic/northern Europe air masses are more pronounced than during other seasons. For the summer months (Fig. 1b, Fig. S3b), the ENA site is dominated by the clean maritime flow associated with the recirculating Azores high. As the recirculating Azores high clusters are usually not associated with long-range transport, a reduced contribution to MBL aerosol from continental pollutions through FT entrainment is expected during the summertime in ENA.

3.2 Mixing ratios of CO, O_3 and water vapor

The mixing ratios of CO, O_3 and water vapor within the MBL are expected to be strongly influenced by entrainment of FT air in ENA. CO is a long-lived species with a lifetime of approximately 1 month (Seinfeld and Pandis, 2016), and therefore is a good indicator of long-range transported continental emissions for remote sites. At the ENA site, the influence of local emissions on trace gases and aerosol measurements is expected to be minimal after filtering of the data (section S1). The lifetime of O_3 varies from hours in polluted urban regions (due to the high rate of photochemical reactions) to several weeks in the FT (Monks et al., 2015). Given its long lifetime in the FT, O_3 may also serve as a tracer for long-range transported pollutants. The local photochemical activities can be inferred from the correlation between O_3 and CO. In regions with strong local sources and sinks, O_3 and CO show a strong positive correlation during summer daytime due to photochemical reactions, but a negative correlation during winter nights due to the stronger dry deposition of O_3 than CO (Poulida et al., 1991; Chin et al., 1994). In contrast, at the ENA site, CO and O_3 are positively correlated all year around, even in winter nighttime with low wind speed (WS) < 2 m/s (Mao and Talbot, 2004) (Fig. S4a). This suggests that the variation of O_3 concentration observed at the ENA site is mainly influenced by the entrainment of FT air, in agreement with findings from previous modeling studies (Cooper et al., 2002; Voulgarakis et al., 2011). In addition, the strong anti-correlation (correlation coefficient being -0.75) of CO and O_3 with water vapor (Fig. S4b) also confirms this picture, as water mixing ratio usually negatively correlates with the extent of FT entrainment at remote marine sites (Helmig et al., 2002). Furthermore, the seasonal variations of O_3 and CO in ENA (Fig. 2a, b) differ much from those observed at anthropogenic-influenced urban or rural sites, where ozone usually exhibits a summer peak due to strong photochemical production, while CO usually shows no clear seasonal variation (Poulida et al., 1991). In contrast, both CO and O_3 in ENA show a summer minimum and spring-winter maximum, which is consistent with the FT entrainment as the dominant source and the seasonal variation of tropopause height. This suggests minor contributions from local emissions and in-situ photochemistry (Parrish et al., 1998; Fischer et al., 2003; Mao and Talbot, 2004). The seasonal variations of CO and O_3 concentrations are also consistent with the cluster analysis of back-trajectories, which indicates more influence from long-range transported pollution in winter-spring than in summer.

3.3 Absorbing aerosols

In the ENA boundary layer, absorbing aerosols, including black carbon, brown carbon, and dust, are likely entrained from the FT following transport from continental sources. Occasionally, air masses with very strong influences from biomass burning or dust are observed at the ENA site. These episodes are excluded from the analyses presented here to focus on the long-term background variations. These episodes are identified using the aerosol optical properties (Logan et al., 2013; Logan et al., 2014; Cazorla et al., 2013), particle chemical compositions (Clarke et al., 2007), and trace gas mixing ratios (Honrath et al., 2004).

Identification of these dust and BB episodes and characterization of aerosol properties during them will be discussed elsewhere (Zheng et al., in prep). With these episodes excluded, the equivalent black carbon (EBC, following the naming convection suggested by Petzold et al. (2013)) mass concentrations were estimated from PM_1 B_{abs} with an assumed mass absorbing cross section of 7.5 $m^2 g^{-1}$ at 529 nm (Bond et al., 2013).

While absorbing particles are entrained from the FT, the seasonal variation of EBC mass concentration is different from those of CO and O_3 (Fig. 2). As evidenced from a decreasing EBC/CO ratio with increasing precipitation rate at cloud base, P_{CB} (Fig. S5), such differences are due to in-cloud coalescence scavenging (section 4.2) both during the long-range transport and/or after entrainment into the MBL, which removes EBC but not CO or O_3. Therefore, EBC mass concentration can be indicative of the overall effect of FT contribution from continental emissions and in-cloud coalescence scavenging. As shown in Fig. 2c, EBC mass concentrations are similar in all seasons, but show larger annual variations than CO or O_3, which are attributed to the larger annual variations of precipitation.

3.4 Aerosol size distributions

3.4.1 Modes of aerosol size distributions

The aerosol size distribution from 70 nm to 1 μm at the ENA site typically consists of three modes (Fig. 3): an Aitken (At) mode below ~ 100 nm, an accumulation mode (Ac) which resides mostly from 100 to 300 nm, and a larger accumulation mode (LA) above ~ 300 nm. Note that due to the lower size limit of UHSAS, the Aitken mode is often not fully characterized. Therefore, its number concentration is derived by deducting fitted number concentrations of the other two modes from the total number concentration *CN* measured by the CPC, namely $N_{At} = CN - N_{Ac} - N_{LA}$. With this definition, the derived Aitken mode concentration also includes nucleation mode particles (i.e., $D_p < 20$ nm). However, previous studies have shown that NPF events within remote MBLs like the ENA are infrequent (Raes, 1995; Bates et al., 2000), therefore nucleation mode particles likely represent a small fraction of the derived Aitken mode number concentration for long term measurements (Wood et al., 2012). The Ac mode is absent in 15 % of cases (Table 2), likely due to in-cloud coalescence scavenging or lack of cloud-processing (section 4). Among these three modes, aerosol number concentration is dominated by At (72.0 %) and Ac (24.9 %) modes (Fig. 3b1), while the volume concentration is controlled by the LA (74.3 %) and Ac (25.1 %) modes (Fig. 3b2). Based on the average volume size distributions (Fig. 3b2) and results shown in Section 5, the LA mode is essentially the sea spray aerosol coarse mode under vast majorities of the conditions.

3.4.2 Seasonal variations of each mode

Different seasonal variations are observed for the three particle modes. While there is substantial variation within each season, on average, the Ac mode exhibits higher number concentration, larger mode D_p, and higher occurrence in summer than in winter (Table 2). In contrast, the LA mode shows opposite seasonal trends, with the number and volume concentrations in winter 1.5 times greater than those in summer (Table 2). These seasonal trends are also evident in the seasonally-averaged size distributions (Fig. 4a). The monthly average concentrations and the seasonal trends of the Ac and LA modes are very consistent from 2015 to 2017, showing little annual variation (Fig. 4b). Despite the higher N_{Ac} in summer, *CN* usually peaks in spring as a result of elevated N_{At} (Fig. 4b). In comparison, the monthly average N_{At} and *CN* exhibit some minor difference among the three years, while their seasonal trends remain the same (Fig. 4b).

4. Governing equation of MBL aerosol number budgets and estimation of the key process terms

4.1 Governing equations of At, Ac, and LA mode concentrations

The mode-dependent seasonal trends indicate that the variations of N_{At}, N_{Ac} and N_{LA} are driven by different processes. Processes that may influence aerosol number concentrations in remote MBL are entrainment of the particles from the FT, SSA production, NPF inside the MBL, condensational growth (COND), coagulation (COAG), in-cloud scavenging of interstitial particles by droplets (INT), aqueous-phase chemistry (AQ_CHEM), wet deposition, dry deposition and advection. Among these processes, NPF within the MBL was shown to be infrequent in previous studies (Raes, 1995; Bates et al., 2000), and is neglected in the calculations of the long-term budget terms (Wood et al., 2012). Also, at remote marine sites like ENA, the influence of advection is "averaged" out for long term trends of particle concentrations. In addition, dry deposition is usually much slower compared to wet deposition for submicron particles, even after taking into account the time and spatial discontinuity of the wet deposition processes (see the discussion of in-cloud scavenging in section 4.2) (Lewis and Schwartz, 2004; Henzing et al., 2006; Wood et al., 2012; Mohrmann et al., 2018). Thus, it is neglected in further analysis. Wet deposition includes both in-cloud coalescence scavenging of activated droplets therefore effectively *CCN* inside clouds (COALES) and the collection of aerosol particles by falling hydrometeors below cloud (i.e., washout). For aerosols between 10 nm and 1 μm, below-cloud washout is usually much less efficient than in-cloud coalescence scavenging (Garrett et al., 2006; Seinfeld and Pandis, 2016; Wood et al., 2012), and is neglected here. Earlier study suggests that the Ac mode in MBL is formed through aqueous-phase chemistry inside cloud droplets (Hoppel et al., 1990). Therefore, we treat both Ac and LA mode particles as *CCN*, and At mode particles as non-*CCN* (i.e., remain as interstitial particles inside clouds). This treatment is also supported by the strong correlation between N_{Ac} + N_{LA} and *CCN* concentration at 0.2 % *ss*, representative for marine low clouds (Leaitch et al., 2010; Wood et al., 2012; Clarke and Kapustin, 2010) during all seasons (Fig. S6). As N_{Ac} is usually one order of magnitude higher than N_{LA} (Fig. 4), the *CCN* concentration at the ENA site is well represented by N_{Ac} alone (Fig. S6). Therefore, the overall governing equation for each mode of MBL aerosol can be written as:

$$\partial_t N_{At} = \partial_t N_{At}\big|_{FT} + \partial_t N_{At}\big|_{SSA} + \partial_t N_{At}\big|_{COND} + \partial_t N_{At}\big|_{COAG} + \partial_t N_{At}\big|_{INT} \quad (1a)$$

$$\partial_t N_{Ac} = \partial_t N_{Ac}\big|_{FT} + \partial_t N_{Ac}\big|_{SSA} + \partial_t N_{Ac}\big|_{COND} + \partial_t N_{Ac}\big|_{COAG} + \partial_t N_{Ac}\big|_{AQ\_CHEM} + \partial_t N_{Ac}\big|_{COALES} \quad (1b)$$

$$\partial_t N_{LA} = \partial_t N_{LA}\big|_{FT} + \partial_t N_{LA}\big|_{SSA} + \partial_t N_{LA}\big|_{COND} + \partial_t N_{LA}\big|_{COAG} + \partial_t N_{LA}\big|_{AQ\_CHEM} + \partial_t N_{LA}\big|_{COALES} \quad (1c)$$

as depicted in Fig. 5 and discussed in detail below.

4.2 Key aerosol sources and sinks

SSA

The change rate of MBL aerosol concentration due to SSA production flux, $\partial_t N|_{SSA}$, can be expressed as (de Leeuw et al., 2011; Wood et al., 2012):

$$\partial_t N\big|_{SSA} = \frac{3.84\times10^{-6}\ \mathrm{WS}^{3.41} F_{SSA}}{H_{MBL}} = \frac{3.84\times10^{-6}\ \mathrm{WS}^{3.41}}{H_{MBL}} \int_{D_p} f_{SSA}\left(lnD_p\right) dlnD_p \quad (2)$$

where 3.84×10^{-6} $\mathrm{WS}^{3.41}$ is the white cap fraction on the sea surface (Monahan et al., 1986) with WS in units of m s^{-1}, F_{SSA} is the total SSA number production flux per white cap area in units of m^{-2} s^{-1}, H_{MBL} is the MBL height in m, and $f_{SSA}(\ln D_p)$ is the

lognormal number size distribution of SSA production flux curve. Thus, WS is the most important parameter in estimating total SSA contributions, while the detailed size distribution could differ with the $f_{SSA}(\ln D_p)$ used (Gong, 2003; Lewis and Schwartz, 2004; Clarke et al., 2006; Grythe et al., 2014).

In-cloud coalescence scavenging

The rate of in-cloud coalescence scavenging of cloud droplets is given by (Wood, 2006; Wood et al., 2012):

$$\partial_t N_d\big|_{COALES} = E\big|_{COALES}\, N_d = -N_d K P_{CB} h H_{MBL}^{-1} \quad (3)$$

where $E|_X$ represents $(\partial_t N|_X)/N$, namely the percentage processing efficiency of process X. N_d is cloud droplet number concentration which is assumed to be the same as *CCN*, or N_{Ac} + N_{LA} (section 3.4.2); K is a constant of 2.25 m^2/kg; while h H_{MBL}^{-1} represents the in-cloud volume fraction of MBL aerosols (MÅrtensson et al., 2010). Note that by letting the precipitation rate at cloud base, P_{CB}, as 0 when there is no precipitation, the precipitation time fraction is already included in Eq. 3.

In-cloud scavenging of interstitial particles by activated droplets

Inside clouds, interstitial particles are scavenged when coagulating with cloud droplets. This process directly reduces At mode particle number concentration, while also indirectly reducing *CCN* (i.e., Ac and LA modes) number concentration by removing particles that could otherwise grow and become *CCN* later (Pierce et al., 2015). The rate of scavenging scales with the probability that the particles are inside clouds, f_{cloud}. Here f_{cloud} is defined as:

$$f_{cloud} = p_{cloud}\, h\, H_{MBL}^{-1}$$

where p_{cloud} is the probability that MBL cloud is encountered and is approximated by the in-cloud time fraction (Table 1), while h H_{MBL}^{-1} is again indicative of the volume fraction of MBL aerosol particles inside the clouds (MÅrtensson et al., 2010).

As At mode particles are treated as non-*CCN* and remain as interstitial particles inside the clouds, the rate of the scavenging can be estimated by (Pierce et al., 2015):

$$\partial_t N_{At}\big|_{INT} = -f_{cloud} K_{int,d} N_{At} N_d, \text{ namely } E\big|_{INT} = -f_{cloud} K_{int,d} N_d \quad (4)$$

where N_d is number concentration of cloud droplets assumed to be the sum of N_{Ac} and N_{LA} (section 3.4.2), $K_{int,\,d}$ is the coagulation coefficient between $D_{p,\,int}$ and $D_{p,\,d}$, where $D_{p,\,int}$ and $D_{p,\,d}$ represent the diameter of interstitial particles and cloud droplets, respectively. $D_{p,\,d}$ is assumed to be 10 μm (Pierce et al., 2015), while $D_{p,\,int}$ is assumed to be the corresponding wet diameter of $D_{pg,\,At}$ under a supersaturation of 0.12 % (Korolev and Mazin, 2003), where $D_{pg,\,At}$ is the geometric mean dry diameter of At mode. The maximum supersaturation near the cloud base where *CCN* activation occurs is typically 0.2 % for marine low clouds (Wood et al., 2012; Clarke and Kapustin, 2010; Leaitch et al., 2010). However, the suspersaturation is usually lower above the cloud base where most of the interstitial scavenging occurs. Here we assume the in-cloud *ss* of 0.12 % based on the work of Korolev and Mazin (2003). Assuming the At mode has a minimum D_p of 23 nm (Pandis et al., 1994), the $D_{pg,\,At}$ is estimated as 48nm, and the corresponding wet particle diameter inside clouds, $D_{p,\,int}$, is around 190 nm. Sensitivity of the interstitial scavenging rate to these parameters is discussed in section 6.3.

Aqueous-phase chemistry

The aqueous-phase reaction (i.e., in-cloud production of sulfate) rate is positively related to the liquid water content (Seinfeld and Pandis, 2016; Meng and Seinfeld, 1994; Pandis et al., 1990; Cheng et al., 2016). As the liquid water content of cloud droplets is orders-of-magnitude higher than that of interstitial aerosols, only aqueous-phase reactions inside the cloud droplets are

considered here (Pandis et al., 1990). As a result, the aqueous-phase reactions only promote the growth of *CCN* (i.e., Ac and LA mode particles). The influence of aqueous-phase reactions on the Aitken mode particles is neglected until they reach *CCN* sizes through condensational growth (Hoppel et al., 1994; Pandis et al., 1990).

Aqueous-phase reactions inside cloud droplets do not change total particle number concentration. On the other hand, it efficiently adds mass to *CCN* and grow them into larger diameters when cloud droplets evaporate following the reactions. Therefore, the only influence of AQ_CHEM on number size distribution considered here is the growth of Ac mode particles into the LA mode size ranges. The magnitude of the influence depends on f_{cloud}, liquid water content, precursor concentrations, and radiation which influences oxidant concentrations (MÅrtensson et al., 2010).

Condensation growth

While condensation does not change the total particle number concentration, it grows the particles and therefore changes the number distribution among different modes (Seinfeld and Pandis, 2016). In this aspect it functions similarly to aqueous-phase reactions, with the difference being that condensation acts on particles of all sizes while aqueous-phase reactions influence only *CCN*. The rate of a smaller mode A growing into a larger mode B through condensation can be estimated as (Pandis et al., 1994):

$$\partial_t N_B\big|_{COND} = -\partial_t N_A\big|_{COND} = (1-f_{cloud})\,J_V(A)/\Delta V_A \quad (5)$$

where ΔV_A (in μm^3) is the volume difference between a particle with the minimum D_p of mode B, and a particle with the volume average of mode A, namely:

$$\Delta V_A = \frac{\pi}{6} D_{p2}{}^3 - \frac{\int_{D_{p1}}^{D_{p2}} \frac{\pi}{6} D_p{}^3 n(D_p) dD_p}{\int_{D_{p1}}^{D_{p2}} n(D_p) dD_p}$$

where the integrals are calculated from the binned aerosol size distribution using the binned-simplification described in Pandis et al. (1994).

J_V (A) is the volume condensation rate of mode A in $\mu m^3\ m^{-3}\ s^{-1}$, which can be estimated as (Seinfeld and Pandis, 2016):

$$J_V(A) = K_{COND}(A)\frac{P}{RT\rho_p} m_i (v_i - v_{eq})$$

where K_{COND} (A) is the condensation rate constant of mode A in s^{-1}, R is the gas constant of 8.314 J mol^{-1}, T is temperature in K, P is the atmospheric pressure being 1.013×10^5 Pa, ρ_p is the aerosol density assumed to be 1×10^{-12} g μm^{-3}, v_i and v_{eq} are the volume mixing ratio of condensate in the bulk gas-phase and at the aerosol surface, and m_i is the molar mass of condensate. Here we assume that the condensate is H_2SO_4 and thus m_i = 98 g mol^{-1}, and v_{eq} is 0 (Pandis et al., 1994). Annual mean v_i is assumed to be 1.0 ppt (Pandis et al., 1994), while being 1.4, 1.3, 1.1 and 0.2 ppt in spring, summer, fall and winter, respectively. This seasonal variation in v_i is based on the monthly dimethyl sulfide (DMS) fluxes (assumed to be 7.0, 5.4, 2.9 and 1.0 µmol m^{-2} day^{-1} in spring, summer, fall and winter, respectively) given in previous studies in the North Atlantic Ocean (Tarrasón et al., 1995), and the proposed dependence of H_2SO_4 on DMS flux at the observed fluxes ranges (Pandis et al., 1994; Russell et al., 1994). Here we assume that H_2SO_4 is the dominant condensate. However, recent studies suggest that organics may play an important role in growth of particles inside the MBL, and this is discussed later in section 6.2.

K_{COND} (A) can be estimated by (Seinfeld and Pandis, 2016):

$$K_{COND}(A) = 2\times10^{-4}\ \pi D\int_{D_{p1}}^{D_{p2}} g_f D_p f(Kn,\alpha) n(D_p) dD_p$$

where 10^{-4} is the unit converter of μm cm^{-1}, D is the gas diffusivity of condensate in air equaling 0.1 cm^2 s^{-1}, g_f is the aerosol hygroscopic growth factor at ambient RH, D_p is the dry aerosol diameter in μm, $n(D_p)$ is the number size distribution of mode A in μm^{-1} cm^{-3}, D_{p1} and D_{p2} are the diameter boundaries of mode A and defined as the corresponding mode gap D_p in Table 2 here, and Kn is the Knudsen number given by $2\lambda_{mfp}$ $(g_f D_p)^{-1}$, where λ_{mfp} is the air mean free path. At the ENA site, observed ambient RH show a modest diurnal variation of 75 % ± 10 %. Accordingly, the hygroscopic growth factor, g_f, is assumed to be 1.3, based on the Hygroscopic Tandem Differential Mobility Analyser measurements of At and Ac mode particles at the ENA site. The increased particle surface area due to hygroscopic growth leads to a factor of ~1.7 increase in the estimated K_{COND} compared with that under dry conditions. The term $f(Kn, \alpha)$ is the correction due to non-continuum effects (scaled by Kn) and imperfect surface accommodation (scaled by the mass accommodation coefficient α) estimated by the Fuchs-Sutugin approach as (Seinfeld and Pandis, 2016):

$$f(Kn,\alpha) = \frac{0.75\alpha(1+Kn)}{Kn^2 + (1+0.283\alpha)Kn + 0.75\alpha}$$

where α is assumed to be 0.02 for H_2SO_4 (Pandis et al., 1994).

Coagulation

Unlike condensation, coagulation does not change the total mass concentration, but reduces aerosol number concentrations. The intra-modal coagulation of particles in a smaller mode A (e.g., At mode) serves as both a source of particles in a larger mode B (corresponding rate denoted as $J_{AA\rightarrow B}$ hereinafter) and a sink for particles of mode A. Given the typical aerosol size distribution observed at the ENA site, intra-modal coagulation of mode A particles is usually negligible when compared to inter-modal coagulation between mode A and another mode B with a different size range (corresponding rate denoted as J_{AB} hereinafter) (Dal Maso et al., 2002). Therefore, we focus on the intra-modal coagulation as a source of a larger mode particles, and inter-modal coagulation as a particle sink. The corresponding rate, $J_{AA\rightarrow B}$ and J_{AB}, are respectively estimated as:

$$J_{AA\rightarrow B} = 0.5\int_{D_{p\min,A}}^{D_{p\max,A}}\int_{D_{pc}}^{D_{p\max,A}} K_{12} n(D_{p1}) n(D_{p2}) dD_{p1} dD_{p2}$$

$$J_{AB} = \int_{D_{p\min,B}}^{D_{p\max,B}}\int_{D_{p\min,A}}^{D_{p\max,A}} K_{12} n(D_{p1}) n(D_{p2}) dD_{p1} dD_{p2}$$

where K_{12} is the coagulation coefficient between two particles with diameters of $g_f D_{p1}$ and $g_f D_{p2}$, respectively, and is calculated using the Fuchs form (Seinfeld and Pandis, 2016). Similarly as in the estimation of K_{COND}, the growth factor under ambient RH, g_f, is assumed to be 1.3. This increase in particle diameter results in a ~20 % decrease in estimated K_{12}. $D_{p\ min,\ A}$ and $D_{p\ max,\ A}$ are the boundary diameter of mode A (defined as the corresponding mode gap D_p in Table 2 here), while $D_{p\ min,\ B}$ and $D_{p\ max,\ B}$ are defined similarly. D_{pc} is defined by

$$D_{pc}^{\ 3} = D_{pB,\ min}^{\ 3} - D_{p1}^{\ 3}$$

The coagulation loss rate of N_A is thus:

$$\partial_t N_A\big|_{COAG} = -(1-f_{cloud})\sum_B J_{AB} \quad (6a)$$

while the coagulation production rate of N_B is:

$$\partial_t N_B\big|_{COAG} = (1-f_{cloud}) J_{AA\rightarrow B} \quad (6b)$$

4.3 Estimated rate of the potential key processes

The terms in the governing equations 1(a-c) due to condensation, coagulation, scavenging of interstitial aerosol, and in-cloud coalescence scavenging of *CCN* are estimated using the equations described above and the size distribution parameters listed in Table 2. The values are listed in Table 3. The discussions of these estimates follow in section 5 and 6.

5 Controlling processes of larger accumulation mode

Potential processes that influence the LA mode number concentration include:

$$\partial_t N_{LA} = \partial_t N_{LA}\big|_{FT} + \partial_t N_{LA}\big|_{SSA} + \partial_t N_{LA}\big|_{COND} + \partial_t N_{LA}\big|_{COAG} + \partial_t N_{LA}\big|_{AQ\_CHEM} + \partial_t N_{LA}\big|_{COALES} \quad (1c)$$

Among these processes, SSA is expected to be the dominant source of N_{LA} in the MBL, as suggested by the strong correlation between N_{LA} and WS (Fig. 6b), a key parameter of SSA production flux (section 4). Aqueous-phase reactions have been reported to produce "droplet mode" particles in the LA mode size range (Pandis et al., 1990; Meng and Seinfeld, 1994). However, if aqueous-phase reactions present a major source, we would expect the volume size distribution to exhibit a mode D_p of 0.6~0.8 μm, corresponding to the size ranges that have the largest access to cloud water (Pandis et al., 1990; Seinfeld and Pandis, 2016). In contrast, the volume size distribution indicates that the LA mode is actually the leading edge of a larger mode with peak D_p in the super-micron range (Fig. 3b2). This is also supported by the strong correlation between V_{LA} and PM_c B_{sca} (Fig. 6c). The PM_c B_{sca} is a surrogate for the supermicron mode (PM_c, D_p 1~10 μm) volume concentration (section 2.2), while supermicron particles are dominated by SSA in remote MBL (Campuzano-Jost et al., 2003). Therefore, the strong correlation suggests that LA particles are also dominated by SSA, and the LA mode is essentially the sea spray aerosol coarse mode under vast majorities of the conditions. The contribution of aqueous-phase reactions to the LA mode number concentration is likely minor, and is neglected from the governing equation Eq. (1c) in following analysis.

Given the large sizes of LA mode particles and that dust and biomass burning episodes are already excluded, we do not expect any significant FT sources. The lack of correlation between N_{LA} and EBC mass concentration also suggests a low concentration of LA mode particles in long-range transported continental pollution plumes. Here we assume that the concentration of LA mode particles in the FT is negligible when compared to that in the boundary layer. In such a case, the entrainment of FT air dilutes the MBL LA particles, serving as a sink rather than a source. At a typical entrainment velocity, ω_e, of 3.5 mm s^{-1} (Mohrmann et al., 2018; Wood and Bretherton, 2004), the maximum dilution rate, $-E_{LA}|_{FT}$, equaling ω_e H_{MBL}^{-1} (Mohrmann et al., 2018), reaches ~ 20 % per day. That is comparable to in-cloud coalescence scavenging, making the FT dilution an important sink of N_{LA}. The sensitivity of the rate to entrainment velocity is discussed at the end of this section.

The terms of intra-modal coagulation ($\partial_t N_{LA}|_{COAG}$) and condensation ($\partial_t N_{LA}|_{COND}$) from the Ac mode are estimated as 0.02 and 0.6 cm^{-3} day^{-1}, respectively (Table 3). Both processes are too slow to exert significant influences on N_{LA} during the typical aerosol lifetime of 7~10 days. The governing equation of N_{LA} (Eq. 1c) can therefore be simplified into:

$$\partial_t N_{LA} = \partial_t N_{LA}\big|_{FT} + \partial_t N_{LA}\big|_{SSA} + \partial_t N_{LA}\big|_{COALES} \quad (7)$$

The seasonal variation of N_{LA} is a result of the balance among the three processes (Fig. 6). Production flux of SSA is proportional to $WS^{3.41}$ H_{MBL}^{-1} (Eq. 2), in-cloud coalescence scavenging efficiency is K P_{CB} h H_{MBL}^{-1} (Eq. 3), and FT dilution efficiency is estimated as ω_e H_{MBL}^{-1}. Among these three terms, the FT entrainment term (Fig. 6e) shows little seasonal variation. In comparison, both the in-cloud coalescence scavenging (Fig. 6d) and the SSA production (Fig. 6f) terms are lower in summer

while higher in winter, with the SSA production exhibiting a stronger seasonal variation. The value of N_{LA} under the quasi-steady-state, (i.e. when $\partial_t N_{LA} = 0$) can be scaled using the three terms for each season. The scaled steady-state N_{LA} (red markers in Fig. 6g) successfully produces the observed seasonal trend of N_{LA} (boxplots and black lines Fig. 6g). Varying the value of the assumed entrainment velocity within the typical range of 2~5 mm s^{-1} does not affect the overall seasonal trend of the scaled N_{LA}.

6. Controlling processes of Aitken - Accumulation mode

6.1 Contributions of SSA to Aitken and Accumulation modes

Unlike N_{LA}, N_{Ac} is independent of the WS, and N_{At} decreases with increasing WS (Fig. 7), indicating relatively minor contributions from SSA to At and Ac modes. The negative correlation between N_{At} and WS may be due to the enhanced N_{LA} with increasing WS (Fig. 6), and thus enhanced coagulation loss for Aitken mode particles (see section 4.2 and section 6.3). In comparison, both N_{At} and N_{Ac} increase monotonically with EBC mass concentration (Fig. 7), suggesting the long-range transported anthropogenic aerosol is a major source of At and Ac mode particles in ENA.

A semi-quantitative estimation of SSA contribution also supports the above conclusion. Assuming all LA mode particles are from SSA, by combining N_{LA} and an established size distribution of SSA production flux, one can estimate the upper limit of the SSA contribution to At and Ac modes (Fig. 8). For simplification, here we use number concentration of particles with D_p in the range from 400 to 1000 nm, N_{400}, to represent the observed SSA number concentration in the same D_p range. SSA larger than ~100 nm are *CCN* under *ss* of 0.1 % (Petters and Kreidenweis, 2007), while the measured *CN* has a cut-off diameter of roughly 10 nm. The contribution of SSA to *CCN* (0.1 %) and CN_{SSA} can therefore be estimated by:

$$CCN(0.1\%)_{SSA} = k_{CCN} N_{400} \frac{\int_{\ln 100}^{\ln 1000} f_{SSA}(\ln D_p) d\ln D_p}{\int_{\ln 400}^{\ln 1000} f_{SSA}(\ln D_p) d\ln D_p} \quad (8a)$$

$$CN_{SSA} = k_{CN} CCN(0.1\%)_{SSA} = CCN(0.1\%)_{SSA}(1 + k_{INT} \frac{\int_{\ln 10}^{\ln 100} f_{SSA}(\ln D_p) d\ln D_p}{\int_{\ln 100}^{\ln 1000} f_{SSA}(\ln D_p) d\ln D_p}) \quad (8b)$$

where k_{CCN} and k_{INT} are factors that account for the size dependence of removal rate (see derivations in SI S3). The estimated k_{CCN} is around 1, while k_{INT} can vary from 1.7 to 4.4 as the removal efficiency is higher for *CCN* than non-*CCN* (Table 4, Fig. 9).

Here we used four published $f_{SSA}(\ln D_p)$ schemes (Gong, 2003; Lewis and Schwartz, 2004; Clarke et al., 2006; Grythe et al., 2014) to calculate the contribution of SSA to observed *CCN*(0.1 %) and *CN* (Fig. 8a). The initial calculation neglects the size dependence of the particle removal rate, therefore the results represent lower limits on the contributions (Fig. 8b). This approach essentially assumes that the shape of the SSA size distribution in the MBL is the same as that of the SSA flux. Even for these lower limit estimates, *CCN* (0.1 %)$_{SSA}$ and CN_{SSA} calculated using $f_{SSA}(\ln D_p)$ from Gong et al. (2003) and Clark et al. (2006) exceed the observed total *CCN* (0.1 %) and *CN* for a substantial fraction of the data, suggesting that these two $f_{SSA}(\ln D_p)$ functions result in overestimation of SSA contributions over the 10-400 nm size range at the ENA site. This may be partially due to the parameter dependencies of sea surface temperatures, etc. (Gantt and Meskhidze, 2013; Gantt et al., 2015; Quinn et al., 2015), which are not considered here. The value of *CCN* (0.1 %)$_{SSA}$ and CN_{SSA} are therefore estimated as the averages of predictions based on flux size distributions reported by Grythe et al (2014) and Lewis and Schwartz (2004), with k_{CCN} and k_{INT} taken into consideration. The corresponding mean fractions of *CCN* (0.1 %)$_{SSA}$ and CN_{SSA} in observed *CCN* (0.1 %) and *CN* are 24 % and 11 %, respectively. The estimated *CCN*(0.1 %)$_{SSA}$ fraction is consistent with a recent study that shows that the SSA

contribution to *CCN* is smaller than 30 % globally (Quinn et al., 2017). In that study, the size distribution of SSA was derived by fitting the aerosol size distribution. If we follow the same approach (Quinn et al., 2017), the estimated SSA number concentration is actually N_{LA} shown in this study, which represents 19 % of *CCN* (0.1 %).

Based on the estimated SSA contribution to *CN* and *CCN* (Eq. 8a and 8b), we can further estimate the SSA contribution to N_{Ac} and N_{At}, $f_{Ac,\,SSA}$ and $f_{At,\,SSA}$, as:

$$f_{Ac,SSA} = (CCN(0.1\%)_{SSA} - N_{LA}) / N_{Ac}$$

$$f_{At,SSA} = (CN_{SSA} - CCN(0.1\%)_{SSA}) / N_{At}$$

and the corresponding annual mean $f_{Ac,\,SSA}$ and $f_{At,\,SSA}$ are 21 % and 10 %, respectively (Table 4).

6.2 Controlling processes of Accumulation mode

As shown in section 6.1, the contribution of SSA to the Ac mode is likely substantial (annual average ~21 %, Table 4). For the Ac mode, both intra-modal and inter-modal coagulations are much slower than in-cloud coalescence scavenging (Table 3), and can therefore be neglected from the governing equation of N_{Ac}. On the other hand, condensational growth of Aitken mode particles may represent a substantial source of the Ac mode. AQ_CHEM reduces N_{Ac} by growing particles into LA size range. As discussed in section 5, this process only makes a minor contribution to N_{LA}. Given N_{Ac} is about one order of magnitude higher than N_{LA}, the impact of AQ_CHEM on N_{Ac} is therefore expected to be negligible. The governing equation of N_{Ac} (Eq. 1b) can be simplified into:

$$\partial_t N_{Ac} = \partial_t N_{Ac}|_{FT} + \partial_t N_{Ac}|_{SSA} + \partial_t N_{Ac}|_{COND} + \partial_t N_{Ac}|_{COALES} \quad (9)$$

The estimated values of $\partial_t N_{Ac}|_{COND}$ and $\partial_t N_{Ac}|_{COALES}$ are listed in Table 3. In-cloud coalescence scavenging is the only sink of Ac mode particles among the four main processes, while the other three are sources. Under steady-state conditions, ($\partial_t N_{Ac}$ =0), we have:

$$f_{SSA,\,Ac} = \frac{\partial_t N_{Ac}|_{SSA}}{\partial_t N_{Ac}|_{FT} + \partial_t N_{Ac}|_{COND} + \partial_t N_{Ac}|_{SSA}} = -\frac{\partial_t N_{Ac}|_{SSA}}{\partial_t N_{Ac}|_{COALES}}$$

Namely

$$\partial_t N_{Ac}|_{SSA} = -f_{SSA,\,Ac}\,\partial_t N_{Ac}|_{COALES}$$

The contribution due to the entrainment of FT air, $\partial_t N_{Ac}|_{FT}$, can be estimated as a residual using the $f_{SSA,\,Ac}$ value derived in the previous section (Table 4):

$$\partial_t N_{Ac}|_{FT} = -(1 - f_{SSA,\,Ac})\,\partial_t N_{Ac}|_{COALES} - E_{Ac}|_{COND} \quad (10)$$

The normalized rates of different processes are compared in Fig. 9a. The derived $\partial_t N_{Ac}|_{FT}$ is stronger in winter-spring while lower in summer-fall, in general agreement with the seasonal trends of observed CO and EBC (Fig. 9b), consistent with the picture that anthropogenic emissions represent the main source of entrained FT Ac mode particles. This agreement also suggests that the above analysis captures the major seasonal variation of the contribution of FT entrainment to Ac mode particles.

Based on the first-order estimates shown in Fig. 9, we can see that on an annual basis, entrainment from the FT represents the major source of N_{Ac}, followed by condensational growth of Aitken mode particles and SSA production. However, the relative importance of these three sources shows substantial seasonal variations. Contributions from SSA production is the lowest in

summer (12 %), and the highest during winter (31 %; Table 4), a result of strong seasonal variation of surface wind speed. In contrast, condensation is negligible in winter due to the substantially lower DMS emissions and thus H_2SO_4 concentrations (section 4.2). In summer and fall, however, the contribution from condensational growth (60 % in summer and 42 % in fall) exceeded that from FT entrainment, and became the dominate source of the Ac mode. This suggests that ocean ecosystems may have a substantial influence on Ac mode particles, and therefore MBL *CCN* populations in ENA. The variation in relative importance despite similar $E_{Ac|COND}$ in spring to fall (Fig. 9a) is mainly due to the large seasonal variation in FT entrainment efficiencies. The estimated contribution from condensation is consistent with observations of individual aerosol particles in the western Atlantic (Sanchez et al., 2018), but is substantially higher than that simulated over the remote Southern Hemisphere oceans during summertime (Hannele et al., 2008). This difference is likely due to the much higher DMS sea surface concentration in ENA (~7.5 nM) than that in the southern oceans (~2.5 nM) (Kettle et al., 1999), or due to the difference between observed and model-simulated aerosol size distributions, etc..

Major uncertainty in the above estimates comes from the concentration of condensates. First, there can be condensates other than H_2SO_4, such as organics. Common biogenic volatile organic compounds (BVOCs) such as isoprene and monoterpenes typically have very low mixing ratio, and SOA formation from these BVOCs is generally minor in the remote marine environment (Kavouras and Stephanou, 2002; Arnold et al., 2009; Gantt et al., 2009; Myriokefalitakis et al., 2010). However, recent studies suggest that photochemistry or heterogeneous oxidation at the sea surface microlayer may represent a substantial source of oxygenated gas-phase organic compounds (OVOCs), which potentially plays an important role in SOA formation and particle growth in the Arctic MBL (Burkart et al., 2017; Willis et al., 2017; Mungall et al., 2017). It is possible that the SOA formation from these OVOCs can contribute to the growth of Aitken mode particles in ENA as well. If so, the contribution to CCN by the growth of Aitken mode particles would be even higher than the estimate here, which is based on condensation of H_2SO_4 only. Second, several studies (Langley et al., 2010; Corbett and Fischbeck, 1997; Capaldo et al., 1999; Corbett et al., 2007; Wang et al., 2008; Johansson et al., 2017) have shown ship emissions represent a significant source of SO_2 in the MBL. In this study, the concentrations of SO_2 and H_2SO_4 are estimated using DMS-SO_2-H_2SO_4 yields based on an observation-based parameterization (Russell et al., 1994; Pandis et al., 1994). Therefore, H_2SO_4 formed from ship emitted SO_2, and its contribution to condensational particle growth is implicitly included.

6.3 Controlling processes of Aitken mode

The governing equation of N_{At} is given by:

$$\partial_t N_{At} = \partial_t N_{At}\big|_{FT} + \partial_t N_{At}\big|_{SSA} + \partial_t N_{At}\big|_{COND} + \partial_t N_{At}\big|_{COAG} + \partial_t N_{At}\big|_{INT} \quad (1a)$$

Following the same approach in Section 6.2, we have:

$$\partial_t N_{At}\big|_{FT} = -(1 - f_{SSA,\,At})(\partial_t N_{At}\big|_{COAG} + \partial_t N_{At}\big|_{COND} + \partial_t N_{At}\big|_{INT}) \quad (11)$$

The contribution of SSA to the Aitken mode is even smaller than it is to the Ac mode, which is estimated to be no larger than 10 % (Table 4). As a result, the entrainment of FT At mode particles represents the dominant source (Fig. 9a). $\partial_t N_{At|FT}$ is higher in spring-summer while lower in fall-winter, and such seasonal variation is somewhat different from those of CO mixing ratio and EBC mass concentrations (Fig. 9b). These differences may be partially due to stronger new particle formation from biogenic precursors in the FT during spring and summer seasons (Sanchez et al., 2018). The strength of new particle formation is not correlated with CO or EBC concentrations, which are tracers for anthropogenic emissions. The contribution of NPF versus

anthropogenic emissions to FT Aitken mode particles cannot be quantitatively determined using data presented here alone, and will be a subject of future study.

On an annual basis, inter-modal coagulation is the major (55 %) sink of N_{At} (Fig. 9), followed by condensation growth (28 %) and interstitial scavenging (16 %). While it is less important when compared to inter-modal coagulation, interstitial scavenging is substantial and cannot be neglected. This is consistent with the finding of Pierce et al. (2015). The overall removal efficiency of N_{At} (~10 % day^{-1}) is substantially lower than those of N_{Ac} and N_{LA}, which corresponds to a longer lifetime (~ 10 days) for At mode particles in MBL. The N_{At} removal efficiency is higher in summer and lower in winter, which is opposite to that of Ac and LA modes. This is partially due to the less efficient removal of At mode particles by coagulation and interstitial scavenging in winter, as a result of lower N_{Ac} and therefore droplet number concentrations. In addition, the low DMS fluxes during winter (section 4.2) lead to substantially weakened condensation growth of At mode particles into Ac mode size ranges, which also contribute to the lower overall removal efficiency in winter. Relative importance of these three removal processes is quite consistent in spring to fall, with contributions from coagulation, condensation and interstitial scavenging being around 51 %, 33 % and 16 %, respectively. In winter, condensation becomes a negligible (7 %) removal processes, while the contribution of coagulation dominates (71 %), with the remaining 22 % due to interstitial scavenging.

We note that there may be some uncertainties in the above estimates, especially the rate of interstitial scavenging, which depends on Aitken mode size distribution, the super-saturation inside clouds, as well as the effective cloud droplet diameters. Based on the assumed baseline conditions (effective cloud droplet diameters of 10 um, average dry interstitial aerosols of 48 nm, and average *ss* of 0.12 %; see section 4.1), relative sensitivities of the $K_{int,\,d}$ are 10 % / μm, -5 % / nm, and -8 % / % with respect to changes in droplet diameter, dry interstitial aerosol diameter, and average *ss*, respectively. For average cloud droplet diameter at 15 μm, geometrical mean Aitken mode diameter of 45 nm and average *ss* of 0.1 %, a condition that is more favorable for intestinal scavenging, corresponding interstitial scavenging rate would increase by a factor of 1.8.

Given the low contribution of SSA to the At mode particles, the governing equation for Aitken mode, Eq. (1a) can be simplified into:

$$\partial_t N_{At} = \partial_t N_{At}\big|_{FT} + \partial_t N_{At}\big|_{COAG} + \partial_t N_{At}\big|_{COND} + \partial_t N_{At}\big|_{INT} \tag{12}$$

7. Conclusion

We examine the seasonal variations of aerosol properties, trace gas mixing ratios, and meteorological parameters measured at the ARM ENA site on Graciosa Island over a three-year period from 2015 to 2017. Aerosol size distributions from 70 nm to 1 μm typically consist of three modes: At (< 100 nm), Ac (100 to ~300 nm) and LA (> 300 nm) modes. Observed *CCN* number concentrations are in general agreement with the sum of N_{Ac} and N_{LA}. The particle number concentration and mode diameter of the three modes exhibits different seasonal variations, suggesting that they are controlled by different processes.

Sources of LA mode particles are dominated by SSA. The major sinks of N_{LA} are in-cloud coalescence scavenging and dilution by entrained FT air. N_{LA} is higher in winter and lower in summer. The higher N_{LA} during winter is attributed to strong SSA production flux due to high wind speed, which prevails over an increase in in-cloud coalescence scavenging. The seasonal

variation of steady-state N_{LA} is derived from scaling the rates of the major processes, and the result agrees well with the observation.

In comparison, SSA represents a relatively minor fraction of N_{Ac} and N_{At}, with estimated annual mean contributions being 21 % and no larger than 10 %, respectively. For N_{Ac}, the other sources are entrained FT Ac mode particles and condensational growth of Aitken mode particle inside the MBL, while the major sink is in-cloud coalescence scavenging. The derived FT contribution to N_{Ac} generally follows the seasonal trends of CO and EBC, namely higher in spring-winter and lower in summer, consistent with the picture that anthropogenic emissions represent the main source of entrained FT Ac mode particles. While entrainment from the FT is the major source on the annual basis, the relative importance of the different sources varies strongly with the season. In summer and fall, condensation growth of the At mode may become the dominant source, contributing 60 % and 42 % of the Ac mode particles in the MBL. In winter, SSA contributes to ~ 31 % of the Ac mode, surpassing the contribution due to condensational growth. This is due to a combination of strong surface wind speed and lower DMS emissions during winter season.

For N_{At}, entrainment from the FT is expected to be the dominant source, and coagulation represents the major sink. The derived FT contribution to N_{At} is higher in spring-summer and lower in fall-winter, possibly due to stronger NPF from biogenic precursors in the FT during spring and summer seasons (Tarrasón et al., 1995). The relative importance of NPF and long-range transported continental emissions to FT Aitken and nucleation mode particles, and the subsequent contribution to the MBL *CCN* population will be examined in future studies. On an annual basis, 52 %, 32 % and 16 % of N_{At} are removed by inter-modal coagulation, condensational growth and interstitial scavenging, respectively. Relative importance of these three removal processes is quite similar from spring to fall. In winter, condensation becomes a negligible (7 %) removal process due to the low DMS fluxes, while contribution of coagulation increases to 71 %.

Based on the above results, the processes that control the concentrations of the different particle modes are summarized in Fig. 10. These results suggest particles entrained from the free troposphere represent the major source of *CCN* in the marine boundary layer. Some of the entrained particles directly contribute to the Ac mode population in the MBL, and are sufficiently large to serve as *CCN*. In addition, Aitken mode particles in the free troposphere, which are attributed to NPF and long-range transported continental emissions, can grow and form *CCN* after their entrainment into the MBL. Our calculation suggests that this represents a significant source of MBL *CCN* all year, with the highest contribution of nearly 60 % during summer seasons. As the growth of Aitken mode particles to *CCN* size is to a large degree the result of the condensation of sulfuric acid, a product of DMS oxidation, this suggests that ocean ecosystems may have a substantial influence on MBL *CCN* population in ENA through emission of DMS.

Acknowledgements

The research was conducted with funding from the Atmospheric System Research (ASR) and Atmospheric Radiation Measurement (ARM) programs (Office of Biological and Environmental Research of US DOE, under contract DE-AC02-98CH10886). We acknowledge the ARM Climate Research Facility, a user facility of the United States Department of Energy (US DOE), Office of Science, sponsored by the Office of Biological and Environmental Research. Robert Wood acknowledges funding from ASR grant DE-SC0013489 (ENA Site Science).

References

Atmospheric Radiation Measurement (ARM) Climate Research Facility. 1990, updated hourly. KAZR Corrected Data (KAZRCORGE). 2015-10-01 to 2018-01-01, Eastern North Atlantic (ENA) Graciosa Island, Azores, Portugal (C1). Compiled by A. Matthews, B. Isom, D. Nelson, I. Lindenmaier, J. Hardin, K. Johnson, N. Bharadwaj, S. Giangrande and T. Toto. Atmospheric Radiation Measurement (ARM) Climate Research Facility Data Archive: Oak Ridge, Tennessee, USA. Data set accessed 2018-03-01 at http://dx.doi.org/10.5439/1350632.

Abdalmogith, S. S., and Harrison, R. M.: The use of trajectory cluster analysis to examine the long-range transport of secondary inorganic aerosol in the UK, Atmospheric Environment, 39, 6686-6695, https://doi.org/10.1016/j.atmosenv.2005.07.059, 2005.

Albrecht, B. A.: Aerosols, Cloud Microphysics, and Fractional Cloudiness, Science, 245, 1227-1230, 10.1126/science.245.4923.1227, 1989.

Albrecht, B. A., Bretherton, C. S., Johnson, D., Scubert, W. H., and Frisch, A. S.: The Atlantic Stratocumulus Transition Experiment—ASTEX, Bulletin of the American Meteorological Society, 76, 889-904, 10.1175/1520-0477(1995)076<0889:taste>2.0.co;2, 1995.

Anderson, T. L., and Ogren, J. A.: Determining Aerosol Radiative Properties Using the TSI 3563 Integrating Nephelometer, Aerosol Science and Technology, 29, 57-69, 10.1080/02786829808965551, 1998.

Arnold, S. R., Spracklen, D. V., Williams, J., Yassaa, N., Sciare, J., Bonsang, B., Gros, V., Peeken, I., Lewis, A. C., Alvain, S., and Moulin, C.: Evaluation of the global oceanic isoprene source and its impacts on marine organic carbon aerosol, Atmos. Chem. Phys., 9, 1253-1262, 10.5194/acp-9-1253-2009, 2009.

Bates, T. S., Quinn, P. K., Covert, D. S., Coffman, D. J., Johnson, J. E., and Wiedensohler, A.: Aerosol physical properties and processes in the lower marine boundary layer: a comparison of shipboard sub-micron data from ACE-1 and ACE-2, Tellus B, 52, 258-272, 10.1034/j.1600-0889.2000.00021.x, 2000.

Blot, R., Clarke, A. D., Freitag, S., Kapustin, V., Howell, S. G., Jensen, J. B., Shank, L. M., McNaughton, C. S., and Brekhovskikh, V.: Ultrafine sea spray aerosol over the southeastern Pacific: open-ocean contributions to marine boundary layer CCN, Atmos. Chem. Phys., 13, 7263-7278, 10.5194/acp-13-7263-2013, 2013.

Bond, T. C., Anderson, T. L., and Campbell, D.: Calibration and Intercomparison of Filter-Based Measurements of Visible Light Absorption by Aerosols, Aerosol Science and Technology, 30, 582-600, 10.1080/027868299304435, 1999.

Bond, T. C., Doherty, S. J., Fahey, D. W., Forster, P. M., Berntsen, T., DeAngelo, B. J., Flanner, M. G., Ghan, S., Kärcher, B., Koch, D., Kinne, S., Kondo, Y., Quinn, P. K., Sarofim, M. C., Schultz, M. G., Schulz, M., Venkataraman, C., Zhang, H., Zhang, S., Bellouin, N., Guttikunda, S. K., Hopke, P. K., Jacobson, M. Z., Kaiser, J. W., Klimont, Z., Lohmann, U., Schwarz, J. P., Shindell, D., Storelvmo, T., Warren, S. G., and Zender, C. S.: Bounding the role of black carbon in the climate system: A scientific assessment, Journal of Geophysical Research: Atmospheres, 118, 5380-5552, 10.1002/jgrd.50171, 2013.

Bony, S., and Dufresne, J.-L.: Marine boundary layer clouds at the heart of tropical cloud feedback uncertainties in climate models, Geophysical Research Letters, 32, n/a-n/a, 10.1029/2005GL023851, 2005.

Bony, S., Colman, R., Kattsov, V. M., Allan, R. P., Bretherton, C. S., Dufresne, J.-L., Hall, A., Hallegatte, S., Holland, M. M., Ingram, W., Randall, D. A., Soden, B. J., Tselioudis, G., and Webb, M. J.: How Well Do We Understand and Evaluate Climate Change Feedback Processes?, Journal of Climate, 19, 3445-3482, 10.1175/jcli3819.1, 2006.

Burkart, J., Hodshire, A. L., Mungall, E. L., Pierce, J. R., Collins, D. B., Ladino, L. A., Lee, A. K. Y., Irish, V., Wentzell, J. J. B., Liggio, J., Papakyriakou, T., Murphy, J., and Abbatt, J.: Organic Condensation and Particle Growth to CCN Sizes in the Summertime Marine Arctic Is Driven by Materials More Semivolatile Than at Continental Sites, Geophysical Research Letters, 44, 10,725-710,734, doi:10.1002/2017GL075671, 2017.

Campuzano-Jost, P., Clark, C. D., Maring, H., Covert, D. S., Howell, S., Kapustin, V., Clarke, K. A., Saltzman, E. S., and Hynes, A. J.: Near-Real-Time Measurement of Sea-Salt Aerosol during the SEAS Campaign: Comparison of Emission-Based Sodium Detection with an Aerosol Volatility Technique, Journal of Atmospheric and Oceanic Technology, 20, 1421-1430, 10.1175/1520-0426(2003)020<1421:nmosad>2.0.co;2, 2003.

Capaldo, K., Corbett, J. J., Kasibhatla, P., Fischbeck, P., and Pandis, S. N.: Effects of ship emissions on sulphur cycling and radiative climate forcing over the ocean, Nature, 400, 743, 10.1038/23438, 1999.

Carslaw, K. S., Lee, L. A., Reddington, C. L., Pringle, K. J., Rap, A., Forster, P. M., Mann, G. W., Spracklen, D. V., Woodhouse, M. T., Regayre, L. A., and Pierce, J. R.: Large contribution of natural aerosols to uncertainty in indirect forcing, Nature, 503, 67, 10.1038/nature12674, 2013.

Cazorla, A., Bahadur, R., Suski, K. J., Cahill, J. F., Chand, D., Schmid, B., Ramanathan, V., and Prather, K. A.: Relating aerosol absorption due to soot, organic carbon, and dust to emission sources determined from in-situ chemical measurements, Atmos. Chem. Phys., 13, 9337-9350, 10.5194/acp-13-9337-2013, 2013.

Cheng, Y., Zheng, G., Wei, C., Mu, Q., Zheng, B., Wang, Z., Gao, M., Zhang, Q., He, K., Carmichael, G., Pöschl, U., and Su, H.: Reactive nitrogen chemistry in aerosol water as a source of sulfate during haze events in China, Science Advances, 2, 10.1126/sciadv.1601530, 2016.

Chin, M., Jacob, D. J., Munger, J. W., Parrish, D. D., and Doddridge, B. G.: Relationship of ozone and carbon monoxide over North America, Journal of Geophysical Research: Atmospheres, 99, 14565-14573, 10.1029/94JD00907, 1994.

Clarke, A., McNaughton, C., Kapustin, V., Shinozuka, Y., Howell, S., Dibb, J., Zhou, J., Anderson, B., Brekhovskikh, V., Turner, H., and Pinkerton, M.: Biomass burning and pollution aerosol over North America: Organic components and their influence on spectral optical properties and humidification response, Journal of Geophysical Research: Atmospheres, 112, n/a-n/a, 10.1029/2006JD007777, 2007.

Clarke, A., and Kapustin, V.: Hemispheric Aerosol Vertical Profiles: Anthropogenic Impacts on Optical Depth and Cloud Nuclei, Science, 329, 1488-1492, 10.1126/science.1188838, 2010.

Clarke, A. D., Owens, S. R., and Zhou, J.: An ultrafine sea-salt flux from breaking waves: Implications for cloud condensation nuclei in the remote marine atmosphere, Journal of Geophysical Research: Atmospheres, 111, n/a-n/a, 10.1029/2005JD006565, 2006.

Clarke, A. D., Freitag, S., Simpson, R. M. C., Hudson, J. G., Howell, S. G., Brekhovskikh, V. L., Campos, T., Kapustin, V. N., and Zhou, J.: Free troposphere as a major source of CCN for the equatorial pacific boundary layer: long-range transport and teleconnections, Atmos. Chem. Phys., 13, 7511-7529, 10.5194/acp-13-7511-2013, 2013.

Cooper, O. R., Moody, J. L., Parrish, D. D., Trainer, M., Ryerson, T. B., Holloway, J. S., Hübler, G., Fehsenfeld, F. C., and Evans, M. J.: Trace gas composition of midlatitude cyclones over the western North Atlantic Ocean: A conceptual model, Journal of Geophysical Research: Atmospheres, 107, ACH 1-1-ACH 1-13, 10.1029/2001JD000901, 2002.

Corbett, J. J., and Fischbeck, P.: Emissions from Ships, Science, 278, 823-824, 10.1126/science.278.5339.823, 1997.

Corbett, J. J., Winebrake, J. J., Green, E. H., Kasibhatla, P., Eyring, V., and Lauer, A.: Mortality from Ship Emissions: A Global Assessment, Environmental Science & Technology, 41, 8512-8518, 10.1021/es071686z, 2007.

Costabile, F., Barnaba, F., Angelini, F., and Gobbi, G. P.: Identification of key aerosol populations through their size and composition resolved spectral scattering and absorption, Atmos. Chem. Phys., 13, 2455-2470, 10.5194/acp-13-2455-2013, 2013.

Dal Maso, M., Kulmala, M., Lehtinen, K. E. J., Mäkelä, J. M., Aalto, P., and O'Dowd, C. D.: Condensation and coagulation sinks and formation of nucleation mode particles in coastal and boreal forest boundary layers, Journal of Geophysical Research: Atmospheres, 107, PAR 2-1-PAR 2-10, 10.1029/2001JD001053, 2002.

de Leeuw, G., Andreas, E. L., Anguelova, M. D., Fairall, C. W., Lewis, E. R., O'Dowd, C., Schulz, M., and Schwartz, S. E.: Production flux of sea spray aerosol, Reviews of Geophysics, 49, n/a-n/a, 10.1029/2010RG000349, 2011.

Dong, X., Xi, B., Kennedy, A., Minnis, P., and Wood, R.: A 19-Month Record of Marine Aerosol–Cloud–Radiation Properties Derived from DOE ARM Mobile Facility Deployment at the Azores. Part I: Cloud Fraction and Single-Layered MBL Cloud Properties, Journal of Climate, 27, 3665-3682, 10.1175/jcli-d-13-00553.1, 2014.

Dong, X., Schwantes, A. C., Xi, B., and Wu, P.: Investigation of the marine boundary layer cloud and CCN properties under coupled and decoupled conditions over the Azores, Journal of Geophysical Research: Atmospheres, 120, 6179-6191, 10.1002/2014JD022939, 2015.

Emeis, S., Jahn, C., Münkel, C., Münsterer, C., and Schäfer, K.: Multiple atmospheric layering and mixing-layer height in he Inn valley observed by remote sensing, Meteorologische Zeitschrift, 16, 415-424, 10.1127/0941-2948/2007/0203, 2007.

Emeis, S., Schäfer, K., and Münkel, C.: Surface-based remote sensing of the mixing-layer height – a review, Meteorologische Zeitschrift, 17, 621-630, 10.1127/0941-2948/2008/0312, 2008.

Eresmaa, N., Karppinen, A., Joffre, S. M., Räsänen, J., and Talvitie, H.: Mixing height determination by ceilometer, Atmos. Chem. Phys., 6, 1485-1493, 10.5194/acp-6-1485-2006, 2006.

Fischer, H., Kormann, R., Klüpfel, T., Gurk, C., Königstedt, R., Parchatka, U., Mühle, J., Rhee, T. S., Brenninkmeijer, C. A. M., Bonasoni, P., and Stohl, A.: Ozone production and trace gas correlations during the June 2000 MINATROC intensive measurement campaign at Mt. Cimone, Atmos. Chem. Phys., 3, 725-738, 10.5194/acp-3-725-2003, 2003.

Gantt, B., Meskhidze, N., and Kamykowski, D.: A new physically-based quantification of marine isoprene and primary organic aerosol emissions, Atmos. Chem. Phys., 9, 4915-4927, 10.5194/acp-9-4915-2009, 2009.

Gantt, B., and Meskhidze, N.: The physical and chemical characteristics of marine primary organic aerosol: a review, Atmos. Chem. Phys., 13, 3979-3996, 10.5194/acp-13-3979-2013, 2013.

Gantt, B., Kelly, J. T., and Bash, J. O.: Updating sea spray aerosol emissions in the Community Multiscale Air Quality (CMAQ) model version 5.0.2, Geosci. Model Dev., 8, 3733-3746, 10.5194/gmd-8-3733-2015, 2015.

Garrett, T. J., Avey, L., Palmer, P. I., Stohl, A., Neuman, J. A., Brock, C. A., Ryerson, T. B., and Holloway, J. S.: Quantifying wet scavenging processes in aircraft observations of nitric acid and cloud condensation nuclei, Journal of Geophysical Research: Atmospheres, 111, n/a-n/a, 10.1029/2006JD007416, 2006.

Gong, S. L.: A parameterization of sea-salt aerosol source function for sub- and super-micron particles, Global Biogeochemical Cycles, 17, n/a-n/a, 10.1029/2003GB002079, 2003.

Grythe, H., Ström, J., Krejci, R., Quinn, P., and Stohl, A.: A review of sea-spray aerosol source functions using a large global set of sea salt aerosol concentration measurements, Atmos. Chem. Phys., 14, 1277-1297, 10.5194/acp-14-1277-2014, 2014.

Haeffelin, M., Angelini, F., Morille, Y., Martucci, G., Frey, S., Gobbi, G. P., Lolli, S., O'Dowd, C. D., Sauvage, L., Xueref-Rémy, I., Wastine, B., and Feist, D. G.: Evaluation of Mixing-Height Retrievals from Automatic Profiling Lidars and Ceilometers in View of Future Integrated Networks in Europe, Boundary-Layer Meteorology, 143, 49-75, 10.1007/s10546-011-9643-z, 2012.

Hannele, K., S., C. K., V., S. D., W., M. G., and T., W. M.: Influence of oceanic dimethyl sulfide emissions on cloud condensation nuclei concentrations and seasonality over the remote Southern Hemisphere oceans: A global model study, Journal of Geophysical Research: Atmospheres, 113, doi:10.1029/2007JD009718, 2008.

Helmig, D., Boulter, J., David, D., Birks, J. W., Cullen, N. J., Steffen, K., Johnson, B. J., and Oltmans, S. J.: Ozone and meteorological boundary-layer conditions at Summit, Greenland, during 3–21 June 2000, Atmospheric Environment, 36, 2595-2608, http://doi.org/10.1016/S1352-2310(02)00129-2, 2002.

Henzing, J. S., Olivié, D. J. L., and van Velthoven, P. F. J.: A parameterization of size resolved below cloud scavenging of aerosols by rain, Atmos. Chem. Phys., 6, 3363-3375, 10.5194/acp-6-3363-2006, 2006.

Honrath, R. E., Owen, R. C., Val Martín, M., Reid, J. S., Lapina, K., Fialho, P., Dziobak, M. P., Kleissl, J., and Westphal, D. L.: Regional and hemispheric impacts of anthropogenic and biomass burning emissions on summertime CO and O3 in the North Atlantic lower free troposphere, Journal of Geophysical Research: Atmospheres, 109, n/a-n/a, 10.1029/2004JD005147, 2004.

Hoppel, W. A., Fitzgerald, J. W., Frick, G. M., Larson, R. E., and Mack, E. J.: Aerosol size distributions and optical properties found in the marine boundary layer over the Atlantic Ocean, Journal of Geophysical Research: Atmospheres, 95, 3659-3686, 10.1029/JD095iD04p03659, 1990.

Hoppel, W. A., Frick, G. M., Fitzgerald, J. W., and Larson, R. E.: Marine boundary layer measurements of new particle formation and the effects nonprecipitating clouds have on aerosol size distribution, Journal of Geophysical Research: Atmospheres, 99, 14443-14459, 10.1029/94JD00797, 1994.

Johansson, L., Jalkanen, J.-P., and Kukkonen, J.: Global assessment of shipping emissions in 2015 on a high spatial and temporal resolution, Atmospheric Environment, 167, 403-415, https://doi.org/10.1016/j.atmosenv.2017.08.042, 2017.

Kavouras, I. G., and Stephanou, E. G.: Particle size distribution of organic primary and secondary aerosol constituents in urban, background marine, and forest atmosphere, Journal of Geophysical Research: Atmospheres, 107, AAC 7-1-AAC 7-12, doi:10.1029/2000JD000278, 2002.

Kettle, A. J., Andreae, M. O., Amouroux, D., Andreae, T. W., Bates, T. S., Berresheim, H., Bingemer, H., Boniforti, R., Curran, M. A. J., DiTullio, G. R., Helas, G., Jones, G. B., Keller, M. D., Kiene, R. P., Leck, C., Levasseur, M., Malin, G., Maspero, M., Matrai, P., McTaggart, A. R., Mihalopoulos, N., Nguyen, B. C., Novo, A., Putaud, J. P., Rapsomanikis, S., Roberts, G., Schebeske, G., Sharma, S., Simó, R., Staubes, R., Turner, S., and Uher, G.: A global database of sea surface dimethylsulfide (DMS) measurements and a procedure to predict sea surface DMS as a function of latitude, longitude, and month, Global Biogeochemical Cycles, 13, 399-444, 10.1029/1999GB900004, 1999.

Korolev, A. V., and Mazin, I. P.: Supersaturation of Water Vapor in Clouds, Journal of the Atmospheric Sciences, 60, 2957-2974, 10.1175/1520-0469(2003)060<2957:sowvic>2.0.co;2, 2003.

Langley, L., Leaitch, W. R., Lohmann, U., Shantz, N. C., and Worsnop, D. R.: Contributions from DMS and ship emissions to CCN observed over the summertime North Pacific, Atmos. Chem. Phys., 10, 1287-1314, 10.5194/acp-10-1287-2010, 2010.

Leaitch, W. R., Lohmann, U., Russell, L. M., Garrett, T., Shantz, N. C., Toom-Sauntry, D., Strapp, J. W., Hayden, K. L., Marshall, J., Wolde, M., Worsnop, D. R., and Jayne, J. T.: Cloud albedo increase from carbonaceous aerosol, Atmos. Chem. Phys., 10, 7669-7684, 10.5194/acp-10-7669-2010, 2010.

Lewis, E. R., and Schwartz, S. E.: Sea salt aerosol production: mechanisms, methods, measurements, and models-A critical review, American geophysical union, 2004.

Liu, Y., and Daum, P. H.: Parameterization of the Autoconversion Process.Part I: Analytical Formulation of the Kessler-Type Parameterizations, Journal of the Atmospheric Sciences, 61, 1539-1548, 10.1175/1520-0469(2004)061<1539:potapi>2.0.co;2, 2004.

Liu, Y., Daum, P. H., McGraw, R., and Wood, R.: Parameterization of the Autoconversion Process. Part II: Generalization of Sundqvist-Type Parameterizations, Journal of the Atmospheric Sciences, 63, 1103-1109, 10.1175/jas3675.1, 2006.

Logan, T., Xi, B., Dong, X., Li, Z., and Cribb, M.: Classification and investigation of Asian aerosol absorptive properties, Atmos. Chem. Phys., 13, 2253-2265, 10.5194/acp-13-2253-2013, 2013.

Logan, T., Xi, B., and Dong, X.: Aerosol properties and their influences on marine boundary layer cloud condensation nuclei at the ARM mobile facility over the Azores, Journal of Geophysical Research: Atmospheres, 119, 4859-4872, 10.1002/2013JD021288, 2014.

Lohmann, U., and Feichter, J.: Global indirect aerosol effects: a review, Atmos. Chem. Phys., 5, 715-737, 10.5194/acp-5-715-2005, 2005.

Mao, H., and Talbot, R.: O3 and CO in New England: Temporal variations and relationships, Journal of Geophysical Research: Atmospheres, 109, n/a-n/a, 10.1029/2004JD004913, 2004.

MÅrtensson, E. M., Tunved, P., Korhonen, H., and Nilsson, E. D.: The role of sea-salt emissions in controlling the marine Aitken and accumulation mode aerosol: a model study, Tellus B, 62, 259-279, 10.1111/j.1600-0889.2010.00465.x, 2010.

Mather, J. H., and Voyles, J. W.: The Arm Climate Research Facility: A Review of Structure and Capabilities, Bulletin of the American Meteorological Society, 94, 377-392, 10.1175/bams-d-11-00218.1, 2013.

Meng, Z., and Seinfeld, J. H.: On the Source of the Submicrometer Droplet Mode of Urban and Regional Aerosols, Aerosol Science and Technology, 20, 253-265, 10.1080/02786829408959681, 1994.

Mohrmann, J., Wood, R., McGibbon, J., Eastman, R., and Luke, E.: Drivers of Seasonal Variability in Marine Boundary Layer Aerosol Number Concentration Investigated Using a Steady State Approach, Journal of Geophysical Research: Atmospheres, 123, 1097-1112, 10.1002/2017JD027443, 2018.

Monahan, E. C., Spiel, D. E., and Davidson, K. L.: A model of marine aerosol generation via whitecaps and wave disruption, in: Oceanic whitecaps, Springer, 167-174, 1986.

Monks, P. S., Archibald, A. T., Colette, A., Cooper, O., Coyle, M., Derwent, R., Fowler, D., Granier, C., Law, K. S., Mills, G. E., Stevenson, D. S., Tarasova, O., Thouret, V., von Schneidemesser, E., Sommariva, R., Wild, O., and Williams, M. L.: Tropospheric ozone and its precursors from the urban to the global scale from air quality to short-lived climate forcer, Atmos. Chem. Phys., 15, 8889-8973, 10.5194/acp-15-8889-2015, 2015.

Morris, V.: Vaisala ceilometer (VCEIL) handbook ARM Climate Research Facility, DOE/SC-ARM-TR-020, 2012.

Müller, T., Laborde, M., Kassell, G., and Wiedensohler, A.: Design and performance of a three-wavelength LED-based total scatter and backscatter integrating nephelometer, Atmos. Meas. Tech., 4, 1291-1303, 10.5194/amt-4-1291-2011, 2011.

Mungall, E. L., Abbatt, J. P. D., Wentzell, J. J. B., Lee, A. K. Y., Thomas, J. L., Blais, M., Gosselin, M., Miller, L. A., Papakyriakou, T., Willis, M. D., and Liggio, J.: Microlayer source of oxygenated volatile organic compounds in the summertime marine Arctic boundary layer, Proceedings of the National Academy of Sciences, 114, 6203-6208, 10.1073/pnas.1620571114, 2017.

Münkel, C., Eresmaa, N., Räsänen, J., and Karppinen, A.: Retrieval of mixing height and dust concentration with lidar ceilometer, Boundary-Layer Meteorology, 124, 117-128, 10.1007/s10546-006-9103-3, 2007.

Myriokefalitakis, S., Vignati, E., Tsigaridis, K., Papadimas, C., Sciare, J., Mihalopoulos, N., Facchini, M. C., Rinaldi, M., Dentener, F. J., Ceburnis, D., Hatzianastasiou, N., O'Dowd, C. D., van Weele, M., and Kanakidou, M.: Global Modeling of the Oceanic Source of Organic Aerosols, Advances in Meteorology, 2010, 16, 10.1155/2010/939171, 2010.

O'Dowd, C. D., and Smith, M. H.: Physicochemical properties of aerosols over the northeast Atlantic: Evidence for wind-speed-related submicron sea-salt aerosol production, Journal of Geophysical Research: Atmospheres, 98, 1137-1149, 10.1029/92JD02302, 1993.

O'Dowd, C. D., Facchini, M. C., Cavalli, F., Ceburnis, D., Mircea, M., Decesari, S., Fuzzi, S., Yoon, Y. J., and Putaud, J.-P.: Biogenically driven organic contribution to marine aerosol, Nature, 431, 676-680, http://www.nature.com/nature/journal/v431/n7009/suppinfo/nature02959_S1.html, 2004.

O'Connor, E. J., Hogan, R. J., and Illingworth, A. J.: Retrieving Stratocumulus Drizzle Parameters Using Doppler Radar and Lidar, Journal of Applied Meteorology, 44, 14-27, 10.1175/jam-2181.1, 2005.

Pandis, S. N., Seinfeld, J. H., and Pilinis, C.: Chemical composition differences in fog and cloud droplets of different sizes, Atmospheric Environment. Part A. General Topics, 24, 1957-1969, https://doi.org/10.1016/0960-1686(90)90529-V, 1990.

Pandis, S. N., Russell, L. M., and Seinfeld, J. H.: The relationship between DMS flux and CCN concentration in remote marine regions, Journal of Geophysical Research: Atmospheres, 99, 16945-16957, 10.1029/94JD01119, 1994.

Parrish, D. D., Trainer, M., Holloway, J. S., Yee, J. E., Warshawsky, M. S., Fehsenfeld, F. C., Forbes, G. L., and Moody, J. L.: Relationships between ozone and carbon monoxide at surface sites in the North Atlantic region, Journal of Geophysical Research: Atmospheres, 103, 13357-13376, 10.1029/98JD00376, 1998.

Petters, M. D., and Kreidenweis, S. M.: A single parameter representation of hygroscopic growth and cloud condensation nucleus activity, Atmos. Chem. Phys., 7, 1961-1971, 10.5194/acp-7-1961-2007, 2007.

Petzold, A., Ogren, J. A., Fiebig, M., Laj, P., Li, S. M., Baltensperger, U., Holzer-Popp, T., Kinne, S., Pappalardo, G., Sugimoto, N., Wehrli, C., Wiedensohler, A., and Zhang, X. Y.: Recommendations for reporting "black carbon" measurements, Atmos. Chem. Phys., 13, 8365-8379, 10.5194/acp-13-8365-2013, 2013.

Phinney, L., Richard Leaitch, W., Lohmann, U., Boudries, H., Worsnop, D. R., Jayne, J. T., Toom-Sauntry, D., Wadleigh, M., Sharma, S., and Shantz, N.: Characterization of the aerosol over the sub-arctic north east Pacific Ocean, Deep Sea Research Part II: Topical Studies in Oceanography, 53, 2410-2433, https://doi.org/10.1016/j.dsr2.2006.05.044, 2006.

Pierce, J. R., Croft, B., Kodros, J. K., D'Andrea, S. D., and Martin, R. V.: The importance of interstitial particle scavenging by cloud droplets in shaping the remote aerosol size distribution and global aerosol-climate effects, Atmos. Chem. Phys., 15, 6147-6158, 10.5194/acp-15-6147-2015, 2015.

Poulida, O., Dickerson, R. R., Doddridge, B. G., Holland, J. Z., Wardell, R. G., and Watkins, J. G.: Trace gas concentrations and meteorology in rural Virginia: 1. Ozone and carbon monoxide, Journal of Geophysical Research: Atmospheres, 96, 22461-22475, 10.1029/91JD02353, 1991.

Prather, K. A., Bertram, T. H., Grassian, V. H., Deane, G. B., Stokes, M. D., DeMott, P. J., Aluwihare, L. I., Palenik, B. P., Azam, F., Seinfeld, J. H., Moffet, R. C., Molina, M. J., Cappa, C. D., Geiger, F. M., Roberts, G. C., Russell, L. M., Ault, A. P., Baltrusaitis, J., Collins, D. B., Corrigan, C. E., Cuadra-Rodriguez, L. A., Ebben, C. J., Forestieri, S. D., Guasco, T. L., Hersey, S. P., Kim, M. J., Lambert, W. F., Modini, R. L., Mui, W., Pedler, B. E., Ruppel, M. J., Ryder, O. S., Schoepp, N. G., Sullivan, R. C., and Zhao, D.: Bringing the ocean into the laboratory to probe the chemical complexity of sea spray aerosol, Proceedings of the National Academy of Sciences, 110, 7550-7555, 10.1073/pnas.1300262110, 2013.

Quinn, P. K., and Bates, T. S.: The case against climate regulation via oceanic phytoplankton sulphur emissions, Nature, 480, 51, 10.1038/nature10580, 2011.

Quinn, P. K., Collins, D. B., Grassian, V. H., Prather, K. A., and Bates, T. S.: Chemistry and related properties of freshly emitted sea spray aerosol, Chem Rev, 115, 4383-4399, 10.1021/cr500713g, 2015.

Quinn, P. K., Coffman, D. J., Johnson, J. E., Upchurch, L. M., and Bates, T. S.: Small fraction of marine cloud condensation nuclei made up of sea spray aerosol, Nature Geosci, advance online publication, 10.1038/ngeo3003 http://www.nature.com/ngeo/journal/vaop/ncurrent/abs/ngeo3003.html#supplementary-information, 2017.

Raes, F.: Entrainment of free tropospheric aerosols as a regulating mechanism for cloud condensation nuclei in the remote marine boundary layer, Journal of Geophysical Research: Atmospheres, 100, 2893-2903, 10.1029/94JD02832, 1995.

Raes, F., Bates, T., McGovern, F., and Van Liedekerke, M.: The 2nd Aerosol Characterization Experiment (ACE-2): general overview and main results, Tellus B: Chemical and Physical Meteorology, 52, 111-125, 10.3402/tellusb.v52i2.16088, 2000.

Rémillard, J., Kollias, P., Luke, E., and Wood, R.: Marine Boundary Layer Cloud Observations in the Azores, Journal of Climate, 25, 7381-7398, 10.1175/jcli-d-11-00610.1, 2012.

Rémillard, J., and Tselioudis, G.: Cloud Regime Variability over the Azores and Its Application to Climate Model Evaluation, Journal of Climate, 28, 9707-9720, 10.1175/jcli-d-15-0066.1, 2015.

Reutter, P., Su, H., Trentmann, J., Simmel, M., Rose, D., Gunthe, S. S., Wernli, H., Andreae, M. O., and Pöschl, U.: Aerosol- and updraft-limited regimes of cloud droplet formation: influence of particle number, size and hygroscopicity on the activation of cloud condensation nuclei (CCN), Atmos. Chem. Phys., 9, 7067-7080, 10.5194/acp-9-7067-2009, 2009.

Russell, L. M., Pandis, S. N., and Seinfeld, J. H.: Aerosol production and growth in the marine boundary layer, Journal of Geophysical Research: Atmospheres, 99, 20989-21003, doi:10.1029/94JD01932, 1994.

Russell, L. M., Hawkins, L. N., Frossard, A. A., Quinn, P. K., and Bates, T. S.: Carbohydrate-like composition of submicron atmospheric particles and their production from ocean bubble bursting, Proceedings of the National Academy of Sciences, 107, 6652-6657, 10.1073/pnas.0908905107, 2010.

Sanchez, K. J., Chen, C.-L., Russell, L. M., Betha, R., Liu, J., Price, D. J., Massoli, P., Ziemba, L. D., Crosbie, E. C., Moore, R. H., Müller, M., Schiller, S. A., Wisthaler, A., Lee, A. K. Y., Quinn, P. K., Bates, T. S., Porter, J., Bell, T. G., Saltzman, E. S., Vaillancourt, R. D., and Behrenfeld, M. J.: Substantial Seasonal Contribution of Observed Biogenic Sulfate Particles to Cloud Condensation Nuclei, Scientific Reports, 8, 3235, 10.1038/s41598-018-21590-9, 2018.

Seinfeld, J. H., and Pandis, S. N.: Atmospheric chemistry and physics: from air pollution to climate change, John Wiley & Sons, 2016.

Springston, S.: Radiance Research Particle Soot/Absorption Photometer Instrument Handbook, DOE ARM Climate Research Facility, Washington, DC (United States), DOE/SC-ARM-TR-176, 2016.

Stein, A. F., Draxler, R. R., Rolph, G. D., Stunder, B. J. B., Cohen, M. D., and Ngan, F.: NOAA's HYSPLIT Atmospheric Transport and Dispersion Modeling System, Bulletin of the American Meteorological Society, 96, 2059-2077, 10.1175/bams-d-14-00110.1, 2015.

Tarrasón, L., Turner, S., and Fløisand, I.: Estimation of seasonal dimethyl sulphide fluxes over the North Atlantic Ocean and their contribution to European pollution levels, Journal of Geophysical Research: Atmospheres, 100, 11623-11639, 10.1029/95JD00849, 1995.

Twomey, S.: Pollution and the planetary albedo, Atmospheric Environment (1967), 8, 1251-1256, https://doi.org/10.1016/0004-6981(74)90004-3, 1974.

Virkkula, A., Ahlquist, N. C., Covert, D. S., Arnott, W. P., Sheridan, P. J., Quinn, P. K., and Coffman, D. J.: Modification, Calibration and a Field Test of an Instrument for Measuring Light Absorption by Particles, Aerosol Science and Technology, 39, 68-83, 10.1080/027868290901963, 2005.

Virkkula, A.: Correction of the Calibration of the 3-wavelength Particle Soot Absorption Photometer (3λ PSAP), Aerosol Science and Technology, 44, 706-712, 10.1080/02786826.2010.482110, 2010.

Voulgarakis, A., Telford, P. J., Aghedo, A. M., Braesicke, P., Faluvegi, G., Abraham, N. L., Bowman, K. W., Pyle, J. A., and Shindell, D. T.: Global multi-year O₃-CO correlation patterns from models and TES satellite observations, Atmos. Chem. Phys., 11, 5819-5838, 10.5194/acp-11-5819-2011, 2011.

Wang, C., Corbett, J. J., and Firestone, J.: Improving Spatial Representation of Global Ship Emissions Inventories, Environmental Science & Technology, 42, 193-199, 10.1021/es0700799, 2008.

Willis, M. D., Köllner, F., Burkart, J., Bozem, H., Thomas, J. L., Schneider, J., Aliabadi, A. A., Hoor, P. M., Schulz, H., Herber, A. B., Leaitch, W. R., and Abbatt, J. P. D.: Evidence for marine biogenic influence on summertime Arctic aerosol, Geophysical Research Letters, 44, 6460-6470, doi:10.1002/2017GL073359, 2017.

Wood, R., and Bretherton, C. S.: Boundary Layer Depth, Entrainment, and Decoupling in the Cloud-Capped Subtropical and Tropical Marine Boundary Layer, Journal of Climate, 17, 3576-3588, 10.1175/1520-0442(2004)017<3576:bldead>2.0.co;2, 2004.

Wood, R.: Drizzle in Stratiform Boundary Layer Clouds. Part I: Vertical and Horizontal Structure, Journal of the Atmospheric Sciences, 62, 3011-3033, 10.1175/jas3529.1, 2005.

Wood, R.: Rate of loss of cloud droplets by coalescence in warm clouds, Journal of Geophysical Research: Atmospheres, 111, n/a-n/a, 10.1029/2006JD007553, 2006.

Wood, R.: Stratocumulus Clouds, Monthly Weather Review, 140, 2373-2423, 10.1175/mwr-d-11-00121.1, 2012.

Wood, R., Leon, D., Lebsock, M., Snider, J., and Clarke, A. D.: Precipitation driving of droplet concentration variability in marine low clouds, Journal of Geophysical Research: Atmospheres, 117, n/a-n/a, 10.1029/2012JD018305, 2012.

Wood, R., Wyant, M., Bretherton, C. S., Rémillard, J., Kollias, P., Fletcher, J., Stemmler, J., Szoeke, S. d., Yuter, S., Miller, M., Mechem, D., Tselioudis, G., Chiu, J. C., Mann, J. A. L., O'Connor, E. J., Hogan, R. J., Dong, X., Miller, M., Ghate, V., Jefferson, A., Min, Q., Minnis, P., Palikonda, R., Albrecht, B., Luke, E., Hannay, C., and Lin, Y.: Clouds, Aerosols, and Precipitation in the Marine Boundary Layer: An Arm Mobile Facility Deployment, Bulletin of the American Meteorological Society, 96, 419-440, 10.1175/bams-d-13-00180.1, 2015.

Wood, R., Stemmler, J. D., Rémillard, J., and Jefferson, A.: Low-CCN concentration air masses over the eastern North Atlantic: Seasonality, meteorology, and drivers, Journal of Geophysical Research: Atmospheres, 122, 1203-1223, 10.1002/2016JD025557, 2017.

Zhou, X., Kollias, P., and Lewis, E. R.: Clouds, Precipitation, and Marine Boundary Layer Structure during the MAGIC Field Campaign, Journal of Climate, 28, 2420-2442, 10.1175/jcli-d-14-00320.1, 2015.

Figures and Tables

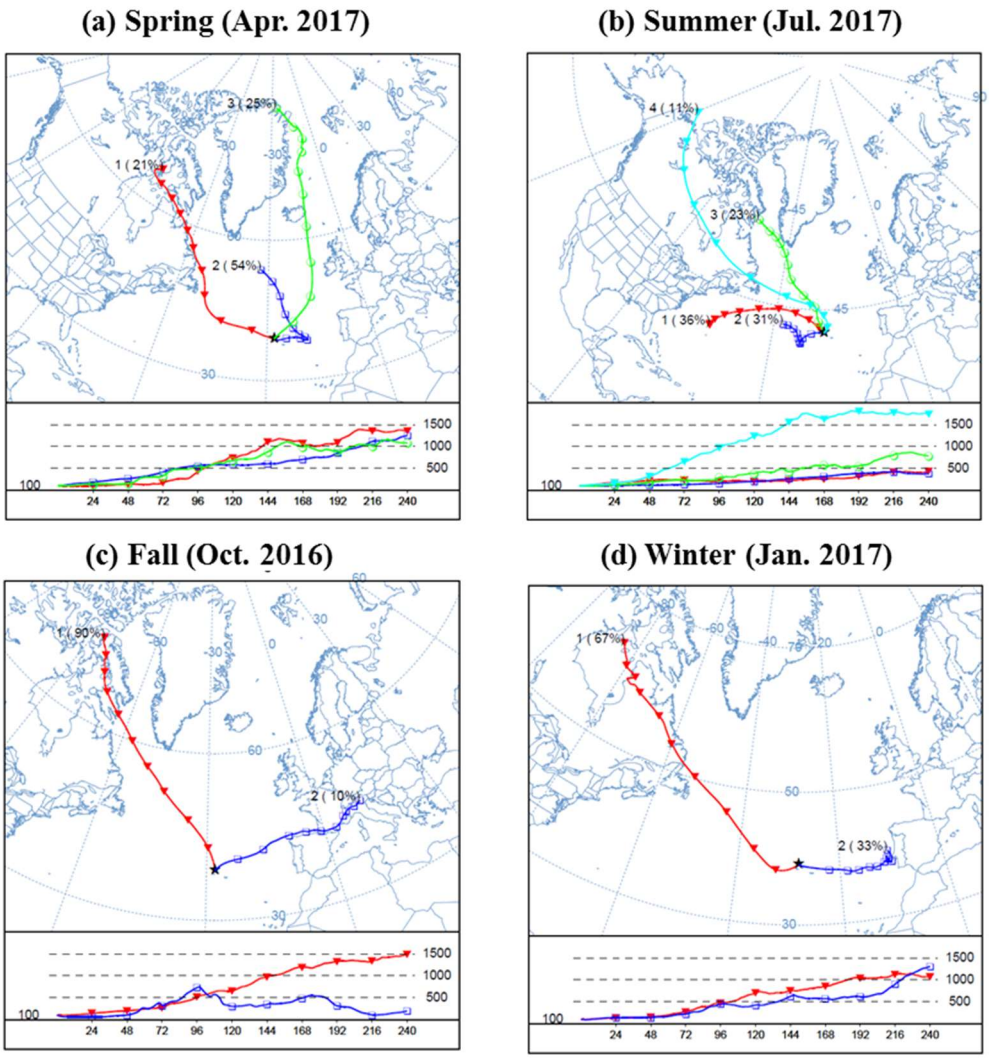

Figure 1. Cluster analysis of 10-day back-trajectories arriving at 100 m above the ENA site in different seasons. The analysis was conducted using the Hybrid Single-Particle Lagrangian Integrated Trajectory (HYSPLIT) 4 model (Stein et al., 2015). The 10-day back trajectories were simulated with a time step of 6 hours using National Centers for Environmental Prediction (NCEP) Global Data Assimilation System (GDAS) meteorological data as input. A cluster analysis of these trajectories was then performed, and for each season, the solution that captures most of the variance (e.g., Abdalmogith and Harrison (2005)) and with less than 5 identified clusters is chosen. The average trajectories of the clusters are represented by different colors, and the associated numbers denoted the arbitrarily given cluster ID and the occurrence percentages of this cluster. For example, number of 1 (90 %) beside the red trajectories indicated that the No. 1 cluster has an average trajectory shown by the red lines, and at 90 % times the air masses arriving at the ENA site belong to this cluster.

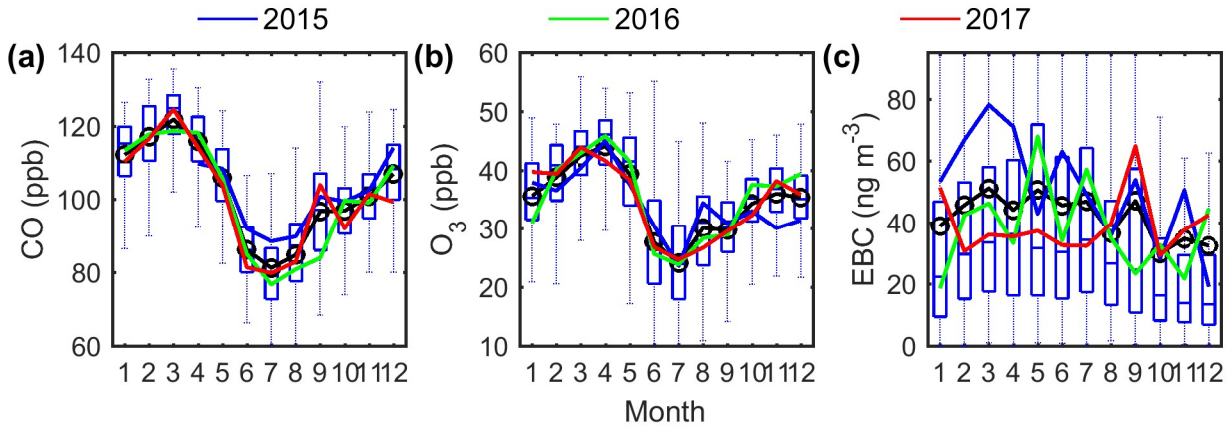

Figure 2. Seasonal variations of (a) CO mixing ratio, (b) O_3 mixing ratio, and (c) EBC concentration at the ENA site. The blue, green, and red lines represent the monthly average for the year 2015, 2016, and 2017, respectively. The whiskers and boxes show the 90th, 75th, median, 25th and 10th percentiles, and the black circle and line represent the mean value of each month for the entire three years.

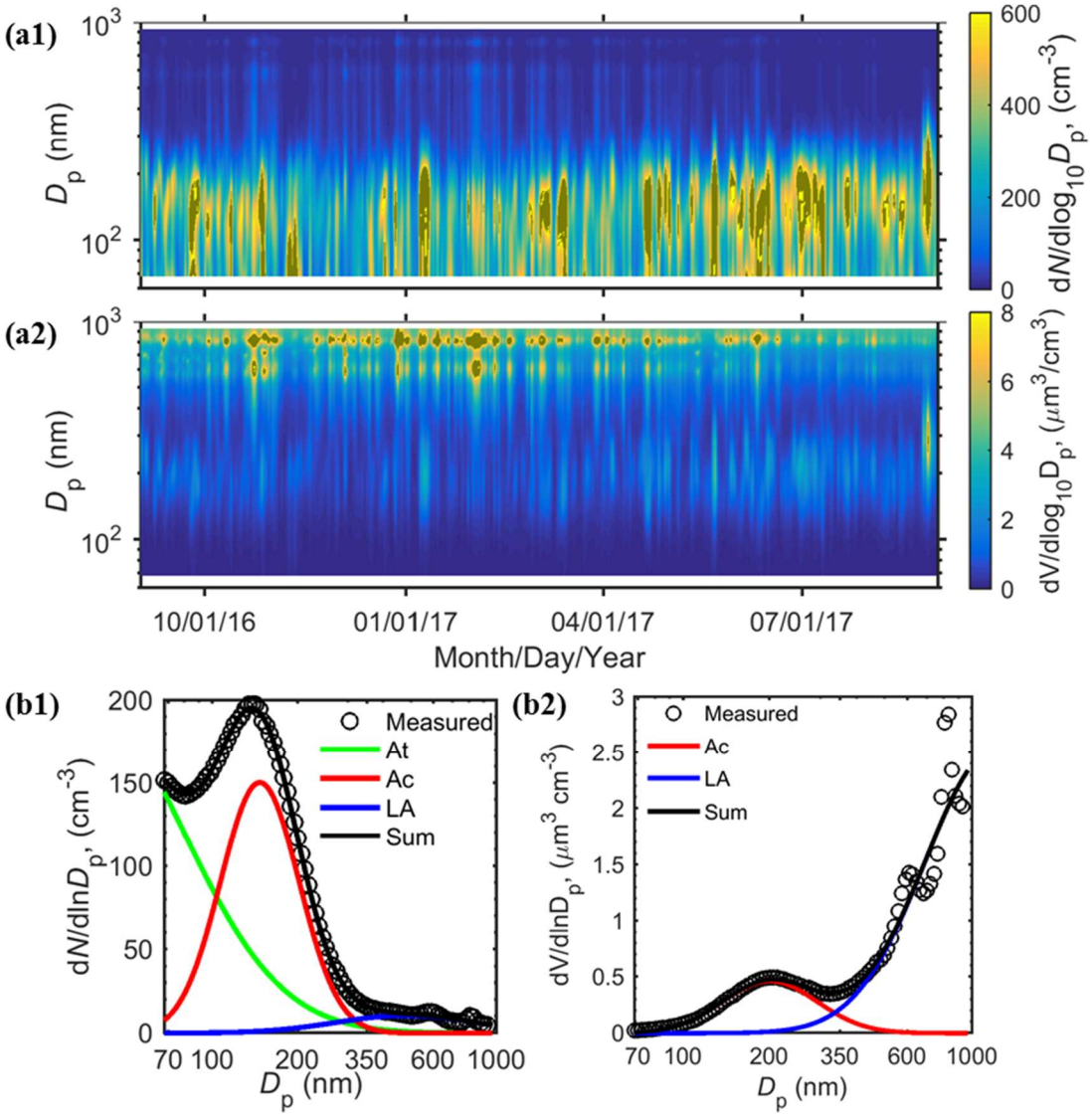

Figure 3. Representative aerosol size distribution measured at the ENA site. Time series of the (a1) number and (a2) volume size distributions during the study period from Sept. 2016 to Aug. 2017, and the fitted lognormal modes of (b1) number and (b2) volume distributions averaged over the one year period. The fluctuations at ~600 nm (also seen in Fig. 4) are considered as instrumental artefacts.

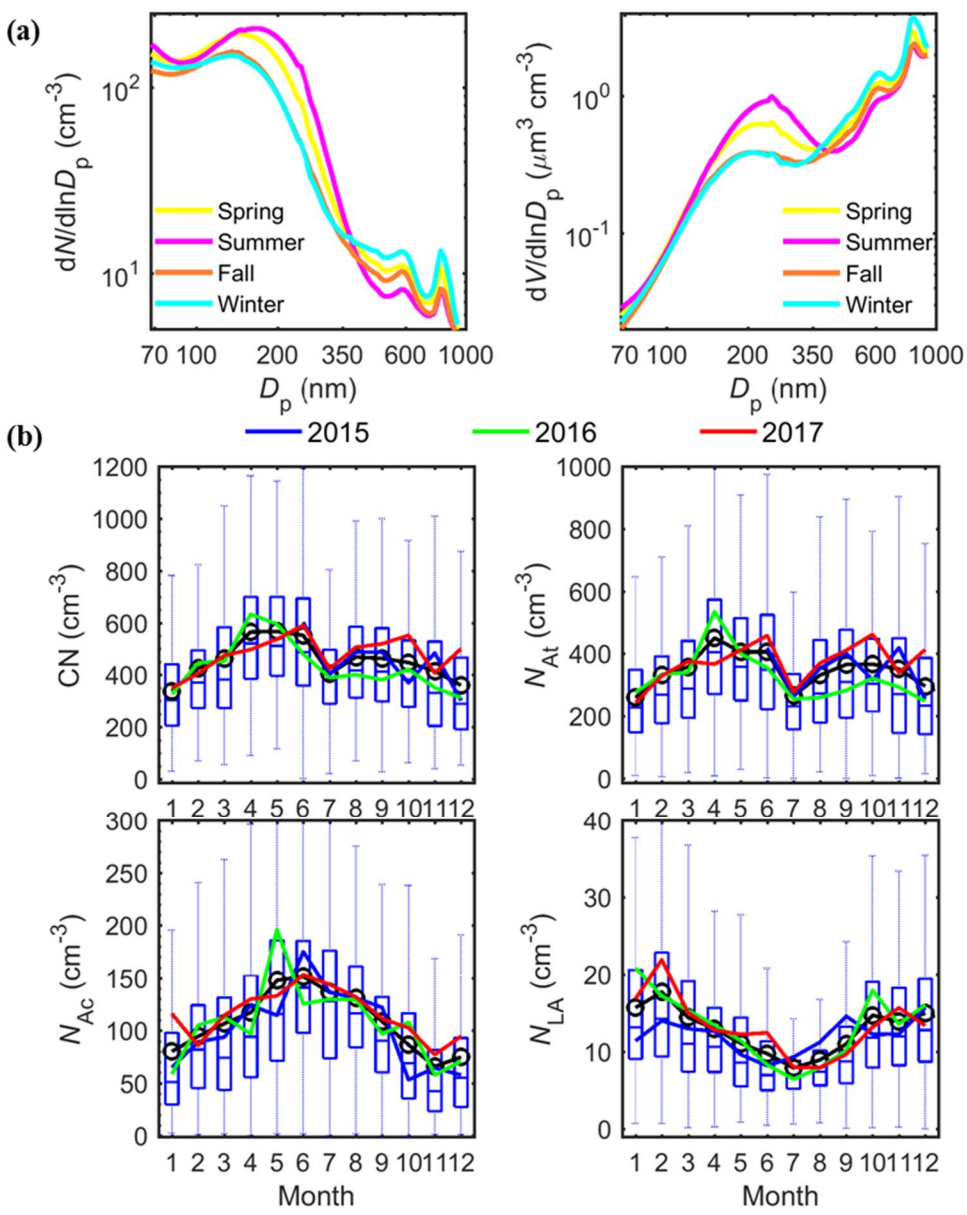

Figure 4: Annual and seasonal variations of aerosol size distributions at the ENA site from 2015 to 2017. (a) Seasonal-averaged number and volume distribution; (b) similar to Fig 2a, but for total aerosol number *CN*, and the number concentrations of At, Ac, and LA modes (N_{At}, N_{Ac} and N_{LA}).

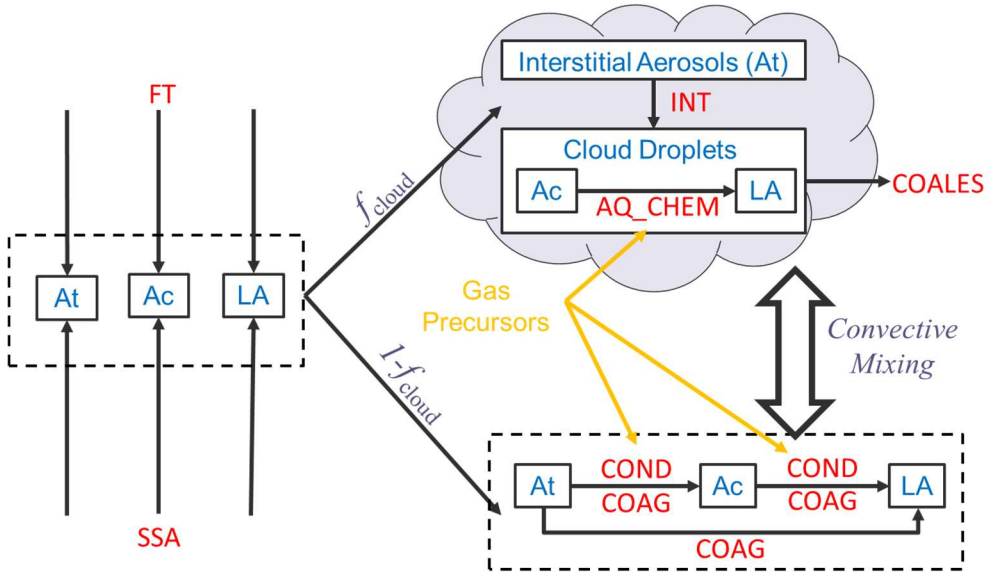

Figure 5. Potential key controlling processes of MBL aerosol number concentrations considered in this study.

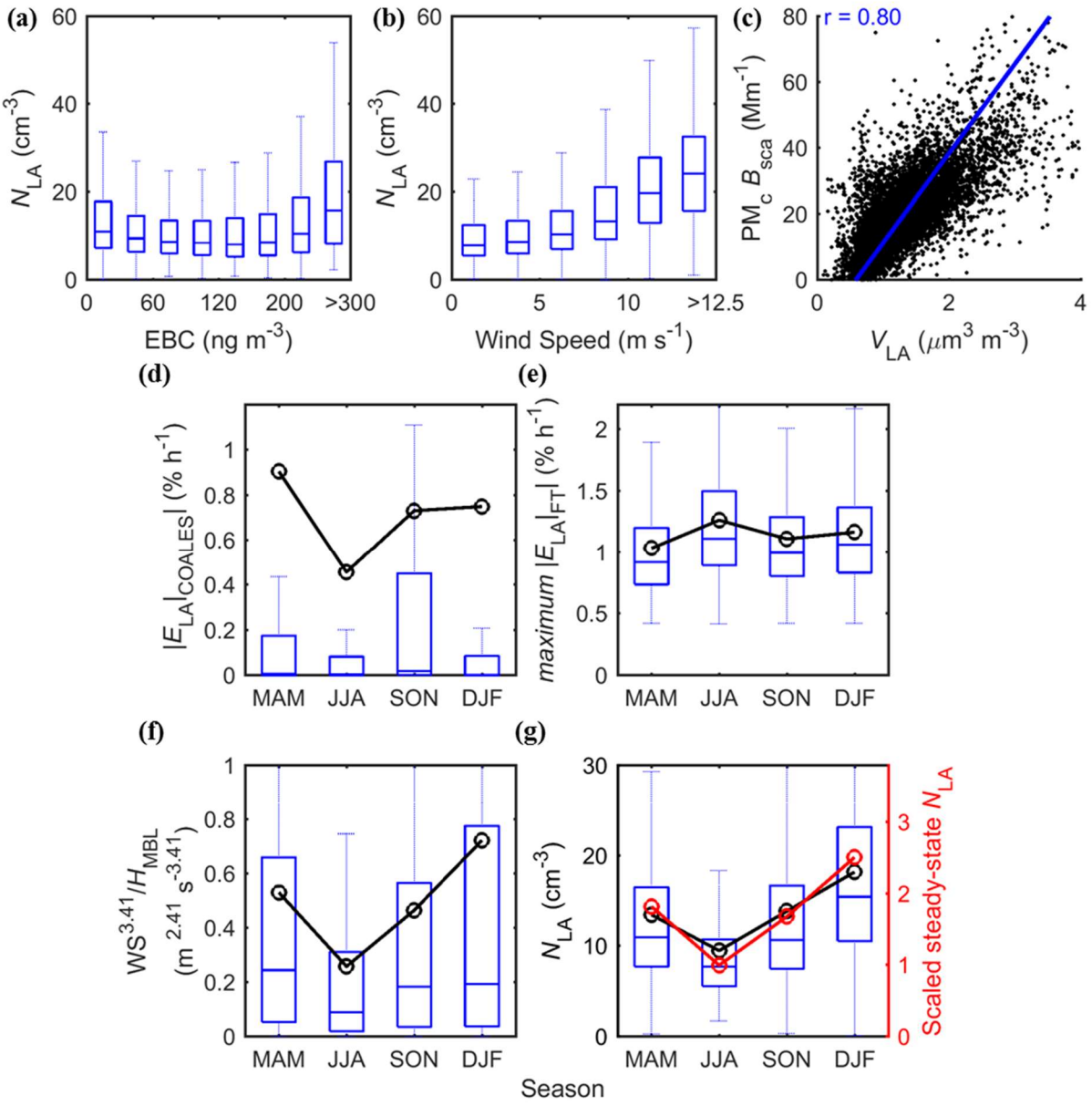

Figure 6. Evidences of key controlling processes of LA mode as SSA and in-cloud coalescence scavenging. (a,b) Dependencies of N_{LA} with EBC and WS for data in 2015 to 2017; (c) correlation between V_{LA} and PM_c B_{sca} for data in 2015 to 2017. The value of r given referred to the Pearson correlation coefficient, while the regression line based on York et al. (2004) is also shown for reference. (d,e) Estimated N_{LA} sinking efficiency due to (d) in-cloud coalescence scavenging and (e) dilution of FT entrainment. (f) Indicators of the major N_{LA} source of SSA, and (g) the corresponding scaled ratios in comparison with observed N_{LA} seasonal patterns. Data shown in (d-g) are from Sept. 2016 to Aug. 2017. The whispers and boxes indicated the 90th, 75th, median, 25th and 10th percentile, respectively. The black circle and lines indicated overall means.

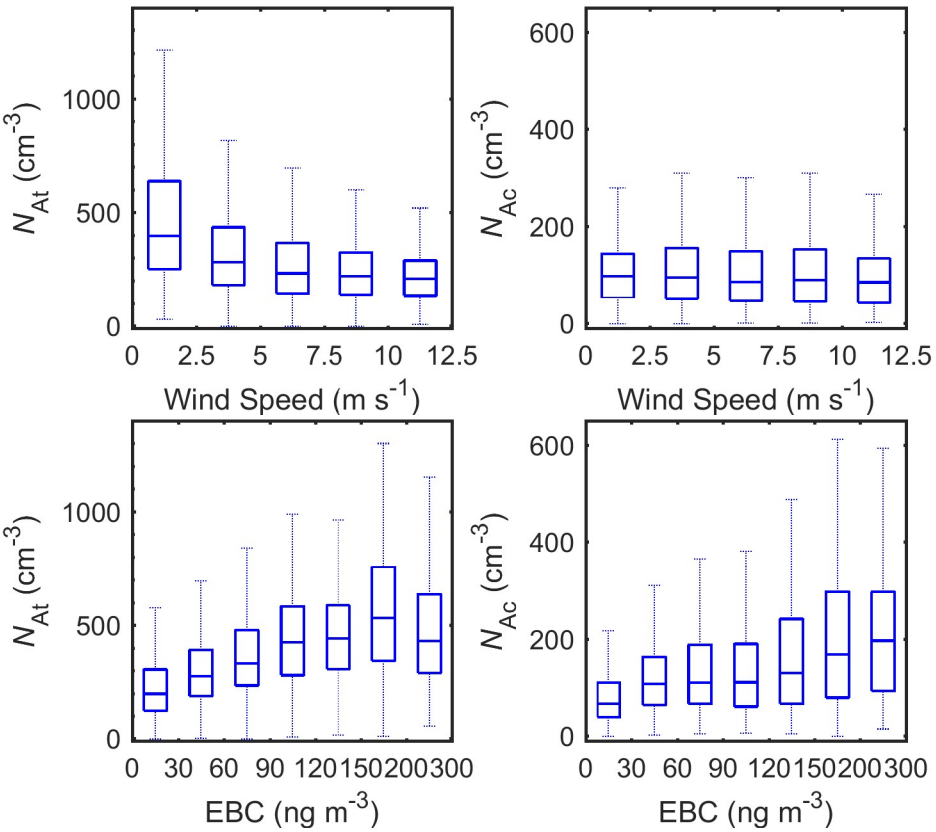

Figure 7. Dependence of N_{At} and N_{Ac} on WS and EBC in 2015 to 2017. The whispers and boxes indicated the 90th, 75th, median, 25th and 10th percentile, respectively.

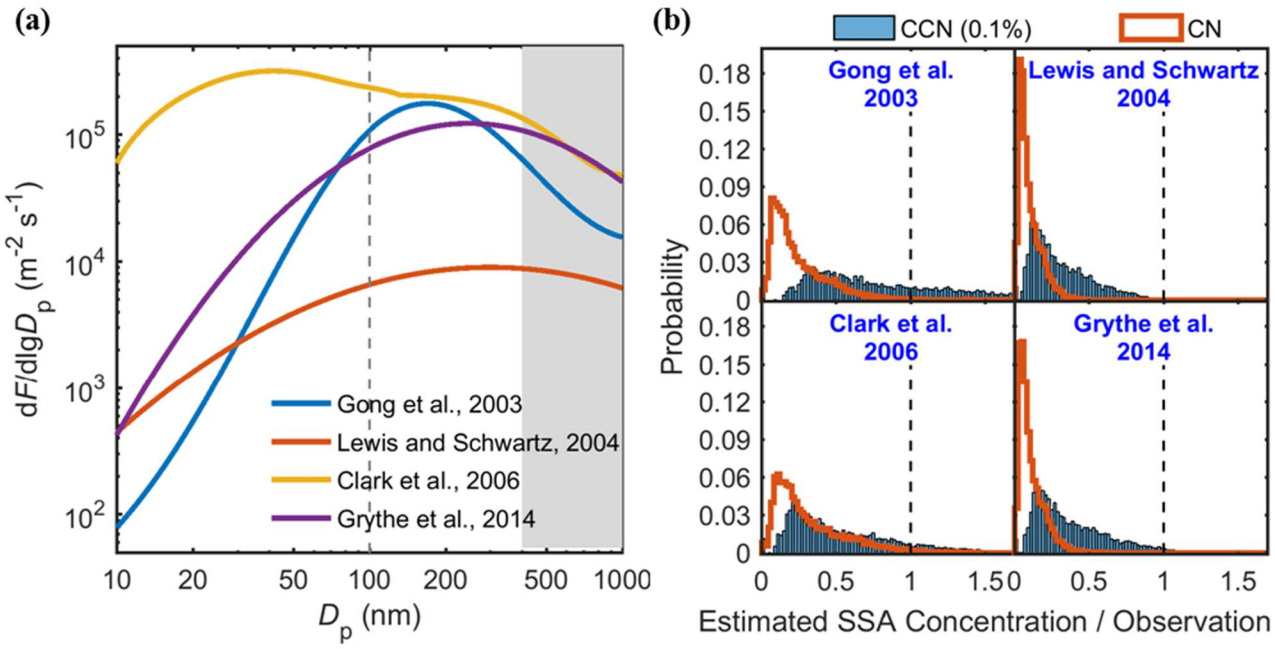

Figure 8. Estimation of SSA contributions to *CN* and *CCN* (0.1%), namely *CCN* concentration at 0.1% supersaturation level. (a) Previously published SSA production flux functions used here, and (b) SSA contribution to observed *CN* and *CCN*(0.1 %) estimated with each of the four SSA production flux functions.

5

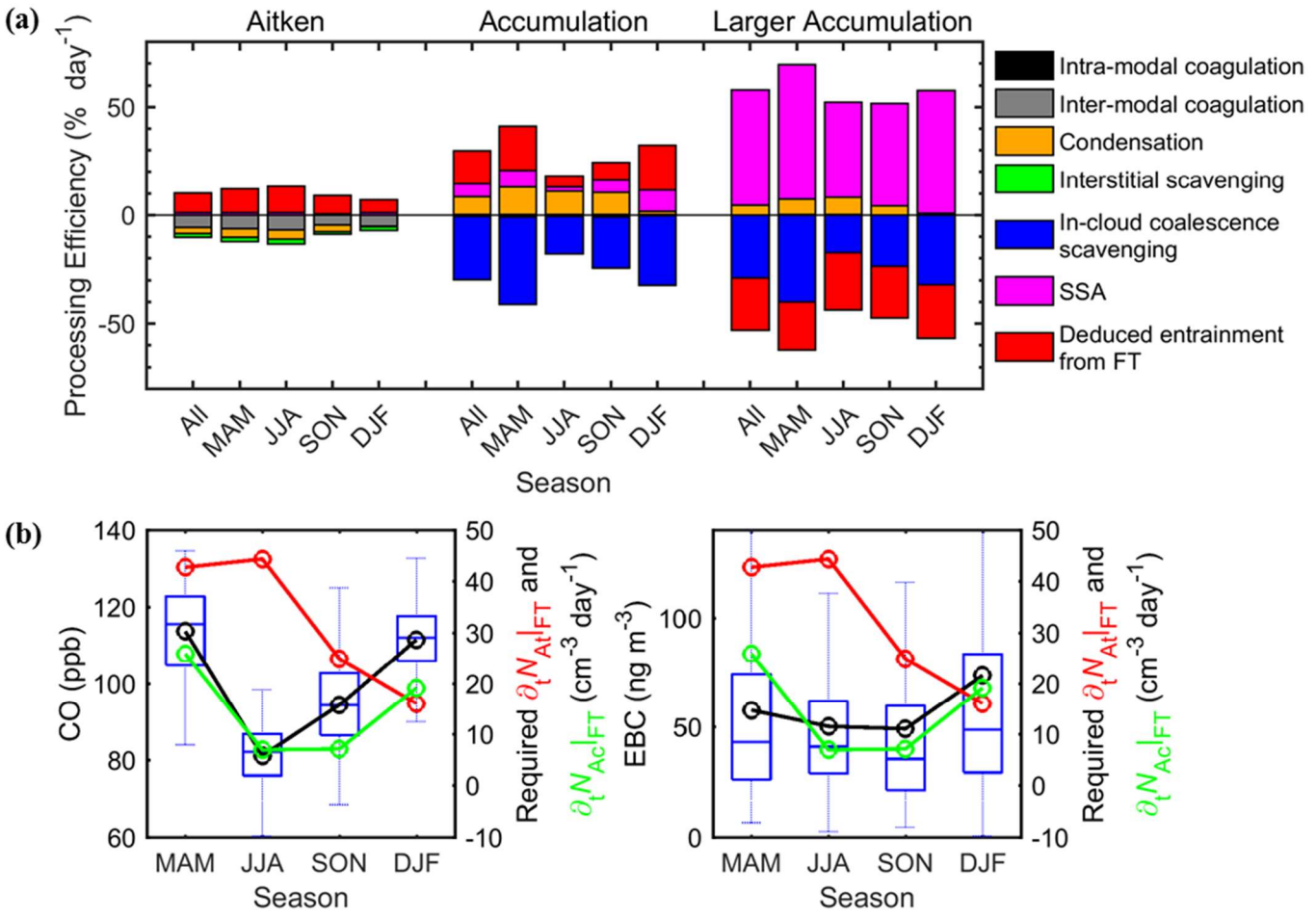

Figure 9. Major controlling processes for each mode. (a) Estimated processing efficiency of each mode in different seasons. (b) Comparison of required seasonal-average FT entrainment rate to N_{At} and N_{Ac}, with CO and EBC. The whispers and boxes indicated the 90th, 75th, median, 25th and 10th percentile, respectively. The black circle and lines indicated overall means.

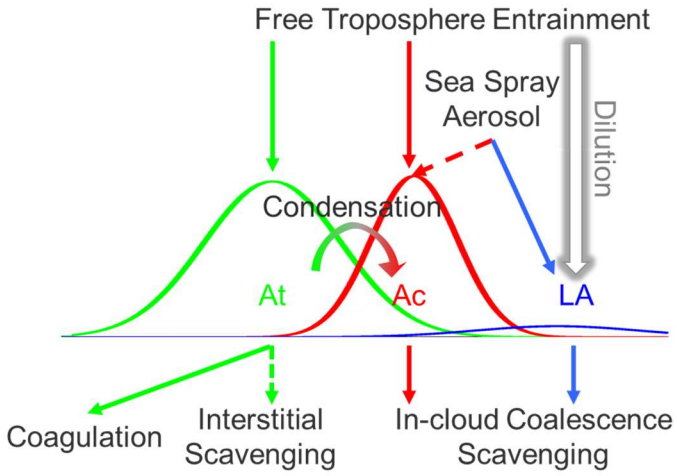

Figure 10. Concept model of key controlling processes of MBL aerosol number concentrations for each mode at ENA. Dash lines indicate the non-dominating but contributing processes. Negligible processes are not shown here.

5

Table 1. Measurements of aerosol and cloud properties at the ENA site used in this study

Measurements	Symbol	Unit	Instruments	Time resolution	Measurement period
Total aerosol number concentration	*CN*	cm^{-3}	Condensation Particle Counter, Model 3772, TSI Incorporated, Shoreview, MN	1 s	Oct. 2013 to Aug. 2014, June 2015 to present
Aerosol number size distribution from 70 nm to 1 μm [a]	$dN/d\ln D_p$	cm^{-3}	Ultra High Sensitivity Aerosol Spectrometer (UHSAS), DMT, Boulder, CO	10 s	Feb. 2014 to present
CCN number concentration at five super-saturations (*ss*)[b]	*CCN* (*ss*)	cm^{-3}	Cloud Condensation Nuclei counter, Model CCN-100, DMT, Boulder, CO	1 s, ss level changes every ~12 min	Oct. 2013 to Apr. 2015, July 2016 to present
Aerosol absorbing coefficient	B_{abs}	Mm^{-1}	3-wavelength Particle Soot Absorption Photometer (3λ-PSAP), Radiance Research, Seattle, WA, USA	1 s for PSAP and 5 s for Nephelometer, inlet upper cut size changes between 1 μm and 10 μm every hour	Oct. 2013 to present
Aerosol scattering coefficient	B_{sca}	Mm^{-1}	Nephelometer, Model 3563, TSI Incorporated, Shoreview, MN		Jan. 2014 to present
Trace gases of CO, NO_2 and H_2O	/	ppb	Gas Analyzer, Model 48C, Thermo Electron Corporation, Franklin, MA	1 s	April 2015 to present
Trace gas of O_3	/	ppb	Ozone monitor, Model 49i, Thermo Fisher Scientific Inc., Franklin, MA	1 s	Oct. 2013 to present
Meteorological parameters [c]	/	/	ENA Aerosol Observing System (AOSMET, DOI: 10.5439/1025153)	1 s	Jan. 2014 to present
MBL height [d]	H_{MBL}	m	Vertically pointing K-band cloud radar (KAZR); Ceilometer, Model CL31, Vaisala, Inc. (North America Support Office), Woburn, MA and Ceilometer CL31	16 s	Dec. 2014 to present
Cloud thickness [d]	*h*	M			
Cloudy time fraction [d]	p_{cloud}	/			
Precipitation rate at cloud base [d]	P_{CB}	$mm\ h^{-1}$		30 min	Oct. 2015 to present

[a] In fact the lower size limit of UHSAS is 60 nm. Here we used only data larger than 70 nm to avoid noises sometimes observed in the first several channels of the UHSAS.

[b] Measured at *ss* levels of 0.1 %, 0.2 %, 0.5 % 0.8 % and 1 %.

[c] Including wind speed (WS) and wind direction (WD), temperature (T), pressure, relative humidity (RH), and rain rate at ground.

[d] See details in section 2.2.2.

Table 2. Statistics of the fitted lognormal mode parameters of the number size distribution measured at the ENA site. The numbers are shown as "mean (standard derivation)" for Sept. 2016 to Aug. 2017 and each of the four seasons during the one year period. Mode D_p and mode σ are the mean and standard deviation of the fitted lognormal distribution of that mode, respectively.

		Annual		Spring (MAM)		Summer (JJA)		Fall (SON)		Winter (DJF)	
Mode N (cm^{-3})	**At**	330	(239)	386	(250)	360	(226)	301	(265)	273	(190)
	Ac	114	(91)	127	(109)	143	(81)	88	(69)	92	(89)
	LA	14	(10)	13	(9)	10	(7)	14	(10)	18	(11)
Mode D_p (nm)	**Ac**	157	(27)	154	(27)	161	(25)	158	(27)	155	(31)
	LA	549	(110)	532	(106)	615	(102)	538	(102)	510	(99)
Mode σ	**Ac**	1.3	(0.3)	1.3	(0.4)	1.3	(0.2)	1.3	(0.3)	1.4	(0.4)
	LA	1.8	(0.7)	1.8	(0.6)	1.8	(0.7)	1.8	(0.7)	1.8	(0.6)
Mode volume ($\mu m^3\ m^{-3}$)	**Ac**	0.3	(0.4)	0.4	(0.3)	0.5	(0.4)	0.3	(0.3)	0.3	(0.4)
	LA	1.1	(0.6)	1.1	(0.4)	0.9	(0.3)	1.1	(0.5)	1.4	(0.7)
Occurrence (%)	**Ac**	85		86		93		86		73	
	LA	83		79		84		84		86	
Mode gap D_p (nm)	**At ~ Ac**	101	(35)	100	(34)	93	(27)	104	(32)	109	(44)
	Ac ~ LA	490	(104)	480	(91)	545	(111)	470	(96)	452	(90)

Table 3. Estimated terms of the governing equations for three modes using size distribution parameters in Table 2[a].

Progress description		Process Rate Quantified	Process Rate (cm^{-3} day^{-1})				
			Annual	Spring (MAM)	Summer (JJA)	Fall (SON)	Winter (DJF)
Intra-modal Coagulation	At+At→Ac	$\partial_t N_{Ac\|COAG}$	0.3	0.4	0.4	0.2	0.2
	Ac+Ac→LA	$\partial_t N_{LA\|COAG}$	0.02	0.02	0.02	0.01	0.01
Inter-modal Coagulation	At+Ac→Ac	$-\partial_t N_{At\|COAG}$	14.1	18.3	20.4	9.8	9.0
	At+LA→LA	$-\partial_t N_{At\|COAG}$	4.5	5.2	3.7	4.1	4.6
	Ac+LA→LA	$-\partial_t N_{Ac\|COAG}$	0.2	0.2	0.2	0.1	0.2
Gas-phase Condensation from H_2SO_4[a]	At→Ac	$-\partial_t N_{At\|COND} = \partial_t N_{Ac\|COND}$	9.5	16.1	15.2	9.1	1.4
	Ac→LA	$-\partial_t N_{Ac\|COND} = \partial_t N_{LA\|COND}$	0.6	0.7	0.6	0.5	0.6
In-cloud Coagulation of Interstitial Aerosol[b]	At→Cloud Droplet (Ac and LA)	$-\partial_t N_{At\|INT}$	5.6	6.8	8.6	3.7	3.9
In-cloud Coalescence Scavenging	Cloud Droplet (Ac and LA)→Drizzling	$-\partial_t N_{Ac\|COALES}$	33.1	50.9	24.6	20.8	29.6
		$-\partial_t N_{LA\|COALES}$	4.0	5.4	1.6	3.3	5.8

[a] Gas-phase H_2SO_4 is assumed to be 1.35 ppt (Pandis et al., 1994); see sensitivity analysis in section 6.2.

Table 4. Parameters and results in estimation of SSA contribution to N_{At} and N_{Ac}.

	Annual			Spring			Summer			Fall			Winter		
$k_{INT,max}$[a]	3.4			4.4			1.7			3.5			4.3		
$f_{SSA,\,Ac}$ (%)	21	±	18	19	±	15	12	±	13	24	±	18	31	±	22
$f_{SSA,\,At}$[a] (%)	10	±	10	9	±	8	8	±	6	7	±	9	16	±	12

[a] Here only an upper limit of k_{INT} without considering the condensation growth is estimated. Correspondingly, the $f_{SSA,\,At}$ is also expected to be an upper limit.

Supporting Information for

Marine boundary layer aerosol in Eastern North Atlantic: seasonal variations and key controlling processes

Guangjie Zheng[1,2], Yang Wang[1,2], Allison C. Aiken[3], Francesca Gallo[3], Michael P. Jensen[1], Pavlos Kollias[4], Chongai Kuang[1], Edward Luke[1], Stephen Springston[1], Janek Uin[1], Robert Wood[5], and Jian Wang[1,2,*]

[1] Environmental and Climate Science Department, Brookhaven National Laboratory, Upton, New York, USA
[2] Center for Aerosol Science and Engineering, Department of Energy, Environmental and Chemical Engineering, Washington University in St. Louis, Missouri, USA
[3] Earth System Observations, Los Alamos National Laboratory, Los Alamos, New Mexico, USA
[4] School of Marine and Atmospheric Sciences, Stony Brook University, State University of New York, Stony Brook, New York, USA
[5] Department of Atmospheric Science, University of Washington, Seattle, USA

Correspondence to: J. Wang (jian@wustl.edu)

S1. Data filtering methods

The Graciosa Airport is located nearby the ENA site, with the east-west extending aircraft runway 116 m north of the site (Wood et al., 2015). Pollution episodes associated with aircraft and road vehicles at Graciosa Airport are identified and screened out based on temporal variation of CN, following a similar method as described in Zheng et al. (2016). Briefly, the change rate of total aerosol number concentration (CN) is calculated first. Subsequently, all time points with change rates larger than 60 cm^{-3} s^{-1}, which is roughly the 95th percentile of all CN change rates, are identified as episode candidates. Starting from these candidates, the program will look forward / backward until all pollution periods is found (Zheng et al., 2016). This method worked satisfactorily as a conservative estimate that can remove the most obvious local pollution periods, which typically constitutes 0 %~20 % of the data within the averaging interval of 1-h.

With this filter, data impacted by local ship emissions are also screened out. Langley et al. (2010) shows that ship particle emissions, when present, can contribute substantially to particle and CCN concentration in the MBL. That condition, if present in ENA, would also be screened out considering the high aerosol number concentration (1000 ~ 3500 cm^{-3}). The contribution of the ship particle emissions averaged over large spatial area in remote marine boundary layer remains unclear, therefore it is not directly treated in this study.

S2. Optical data corrections

B_{abs} can be derived by Bond's correction of: $B_{abs} = B_{PSAP}$ - 0.0164 B_{NEPH} (Bond et al., 1999). For this purpose, conversion of B_{NEPH} from Nephelometer measurement wavelengths (450, 550, and 700 nm) to 3λ-PSAP measurement wavelengths (464, 529, and 648 nm) is needed, through interpolation based on the Scattering Ångström Exponent (SAE) (Costabile et al., 2013). For example, B_{NEPH} at 529 nm are derived by:

$$SAE_{NEPH}(550) = -\frac{\log(B_{NEPH}(700)/B_{NEPH}(450))}{\log(700/450)}, \text{ and } B_{NEPH}(529) = B_{NEPH}(550)\,[(\frac{529}{550})^{-SAE_{NEPH}(550)}]$$

where the numbers in parenthesis denoted the wavelengths in nm. Similarly, B_{NEPH} at 464 and 648 nm were derived from those measured at from 450 and 700 nm, using SAE derived by 450 nm /550 nm and 550 nm /700 nm wavelength pairs. Note that there's another correction method proposed by Virkkula et al. (Bond et al., 1999; Virkkula et al., 2005; Virkkula, 2010). Based on our data, that correction will result in a 6 % lower value in B_{abs} at 529 nm, but showing the same trend with Bond' correction (R^2=0.99). As here we only discussed about relative trends in B_{abs} here, the detailed correction method would not influence our conclusions.

For B_{sca}, truncation and angular illumination corrections using SAE are applied, following the method proposed by Anderson and Ogren (1998). Briefly, that is $B_{sca} = (a+b\cdot SAE)\cdot B_{NEPH}$, where the wavelength-dependent correction coefficient $a(\lambda)$ and $b(\lambda)$ are taken from Müller et al. (2011), with the "sub-μm" and "no cut" coefficients applied for PM_1 and PM_{10} signals, respectively. After this correction, B_{sca} is further converted to PSAP-corresponding wavelengths through the SAE interpolation method as described above. Again, take data at 529 nm for example, it was derived by:

$$SAE(550) = -\frac{\log(B_{sca}(700)/B_{sca}(450))}{\log(700/450)}, \text{ and } B_{sca}(529) = B_{sca}(550)\,[(\frac{529}{550})^{-SAE(550)}]$$

S3. Estimation of k_{CCN} and k_{CN}

For $CCN(0.1\ \%)_{SSA}$, the influence of secondary processing is expected to be negligible. SSA over 100 nm would all have been activated under typical cloud *ss*, thus the ratio of $CCN(0.1\ \%)_{SSA}$ to N_{400} would be conserved during coalescence scavenging. Non-cloud processing would reduce N_{Ac} through coagulation loss, while this influence is expected to be small (section 6.2, Table 3). Thus we have $k_{CCN} = 1$.

In terms of *CN*, the situation could be more complicated since it includes both *CCN* and interstitial aerosols. Coalescence scavenging would reduce $CCN(0.1\ \%)_{SSA}$ without impacting the interstitial aerosols, thus elevating actual $CN/CCN(0.1\ \%)_{SSA}$ ratio and underestimating the CN_{SSA}. To the contrary, coagulation loss and interstitial scavenging could be a major non-*CCN* loss term (section 6.2, Table 3), which will result in a lower actual $CN/CCN(0.1\ \%)_{SSA}$ ratio than theoretically predicted, and thus an overestimation in estimated CN_{SSA}. The overall influence depends on the relative strength of these two mechanisms. Assuming that both the $CCN(0.1\ \%)_{SSA}$ and the interstitial aerosols from SSA, $N_{INT,\ SSA}$, are in steady state (namely $\partial_t CCN(0.1\ \%)_{SSA} = 0$ and $\partial_t N_{INT,\ SSA} = 0$), then we have:

$$\int_{\ln 100}^{\ln 1000} f_{SSA}(\ln D_p) d\ln D_p = (E_{CCN}|_{PRCP} + E_{CCN}|_{COND} + E_{CCN}|_{FT,dilute}) CCN(0.1\%)_{SSA}$$

$$\int_{\ln 10}^{\ln 100} f_{SSA}(\ln D_p) d\ln D_p = (E_{CN-CCN}|_{INT} + E_{CN-CCN}|_{COAG} + E_{CN-CCN}|_{COND} + E|_{FT,dilute}) N_{INT,SSA}$$

$$= (E_{CN-CCN}|_{INT} + E_{CN-CCN}|_{COAG} + E_{CN-CCN}|_{COND} + E|_{FT,dilute})(CN_{SSA} - CCN(0.1\%)_{SSA})$$

where $E|_{FT,dilute}$ is the dilution efficiency of FT air being $-\omega_e/H_{MBL}$ (section 5). Combing these two equations, we have:

$$\frac{CN_{SSA} - CCN(0.1\%)_{SSA}}{CCN(0.1\%)_{SSA}} = \frac{E_{CCN}|_{COALES} + E_{CCN}|_{COND} + E|_{FT,dilute}}{E_{CN-CCN}|_{INT} + E_{CN-CCN}|_{COAG} + E_{CN-CCN}|_{COND} + E|_{FT,dilute}} \frac{\int_{\ln 10}^{\ln 100} f_{SSA}(\ln D_p) d\ln D_p}{\int_{\ln 100}^{\ln 1000} f_{SSA}(\ln D_p) d\ln D_p}$$

Thus k_{INT} could be estimated by:

$$k_{INT} = \frac{E_{CCN}|_{COALES} + E_{CCN}|_{COND} + E|_{FT,dilute}}{E_{CN-CCN}|_{INT} + E_{CN-CCN}|_{COAG} + E_{CN-CCN}|_{COND} + E|_{FT,dilute}} < \frac{E_{CCN}|_{COALES}}{E_{CN-CCN}|_{INT} + E_{CN-CCN}|_{COAG}}$$

The estimated coalescence scavenging efficiency (17 % ~ 40 % CCN day^{-1}) is 1.7-4.4 times stronger than the overall efficiency of coagulation loss and interstitial scavenging (Table 3). Correspondingly, the upper limit of k_{INT} is expected to be between 1.7 and 4.4 (Table 4).

Fig. S1 to S6

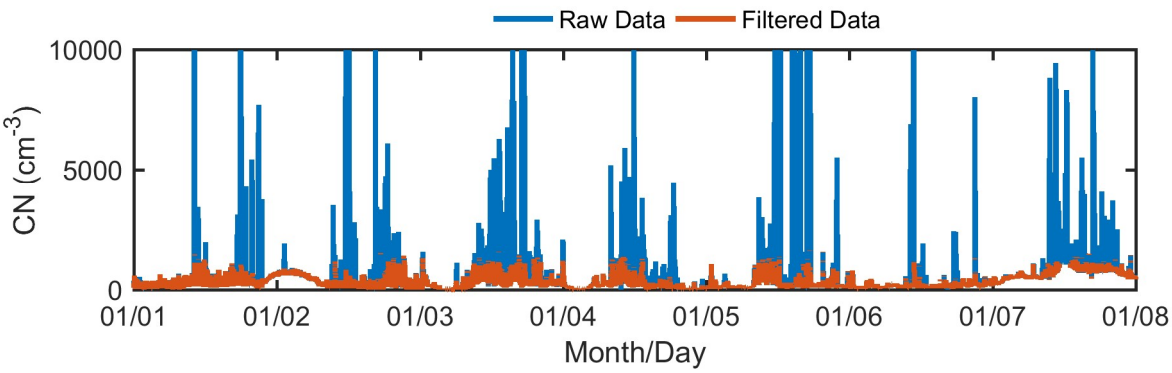

Figure S1. Raw and filtered CN during the first week in Jan. 2017, as an example of the outcome of the pollution episode filtering method used here.

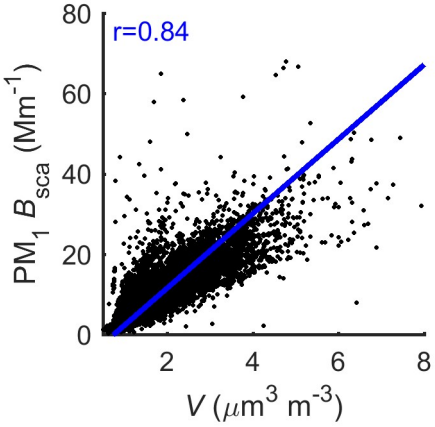

Figure S2. Correlation of PM_1 B_{sca} and total volume concentration derived from UHSAS measurements from 2015 to 2017. The value of *r* given referred to the Pearson correlation coefficient, while the regression line based on York et al. (2004) is also shown for reference.

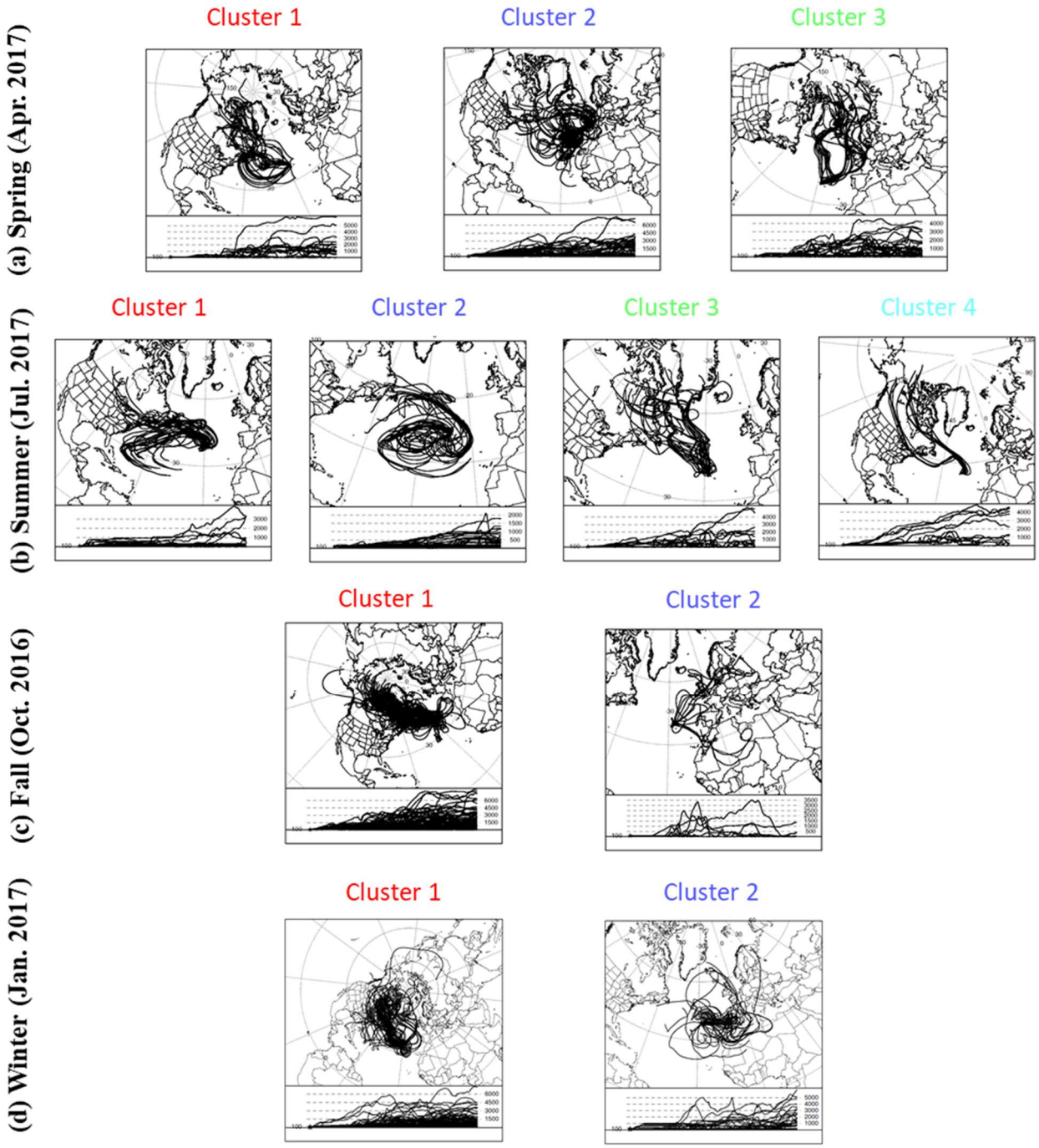

Figure S3. Detailed trajectories for each cluster shown in Fig. 1.

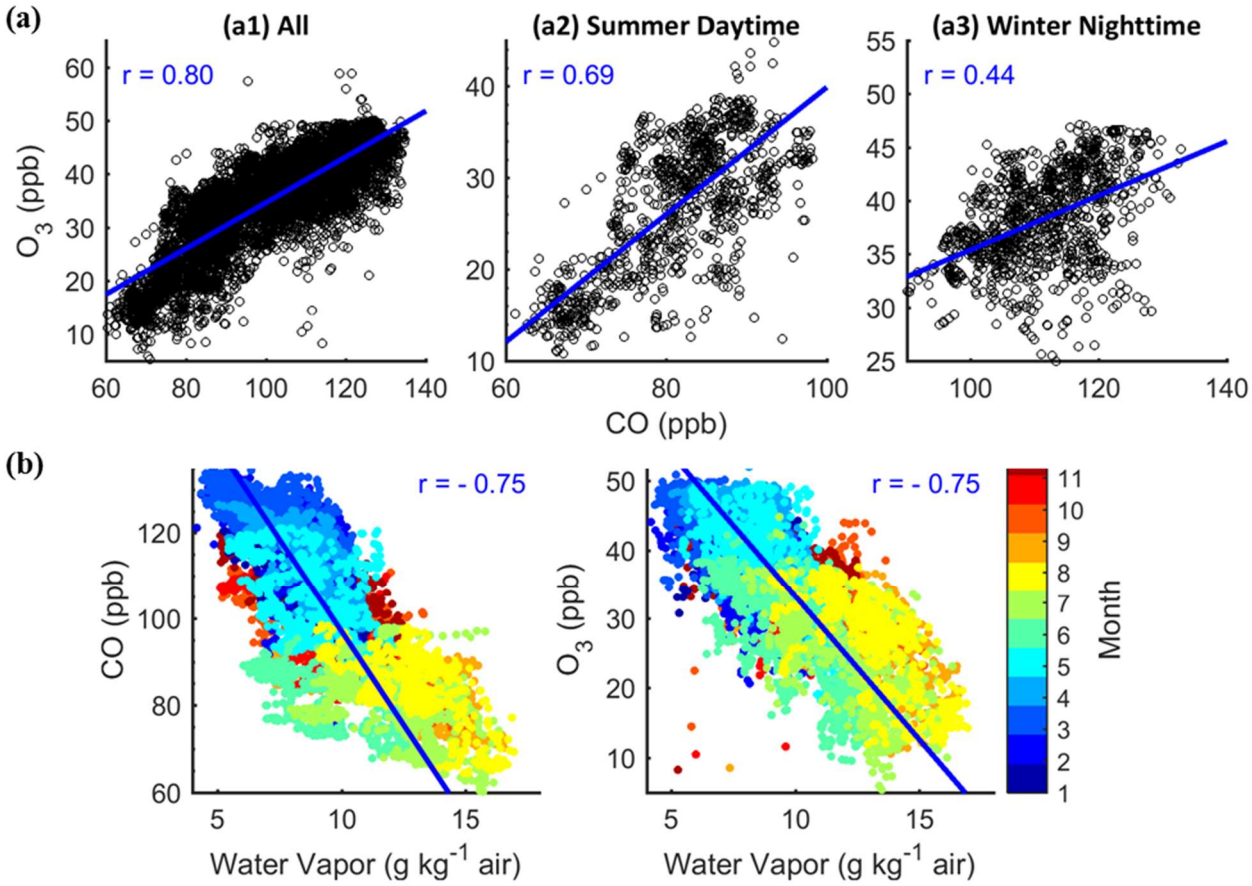

Figure S4. Evidences of FT domination on ENA CO and O_3. (a) O_3-CO correlations during (a1) all periods, (a2) summer daytime and (a3) winter nighttime, where daytime indicated 8:00 to 20:00 LT. (b) Correlation of CO and O_3 with water vapor. Data during the identified dust and biomass burning episodes (section 3.3) is excluded here. The value of r given referred to the Pearson correlation coefficient, while the regression line based on York et al. (2004) is also shown for reference.

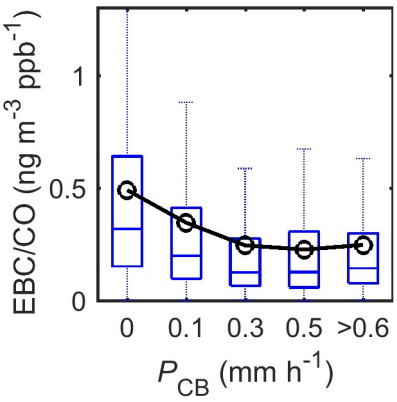

Figure S5. Dependence of EBC to CO ratio with precipitation rate at cloud base (P_{CB}).

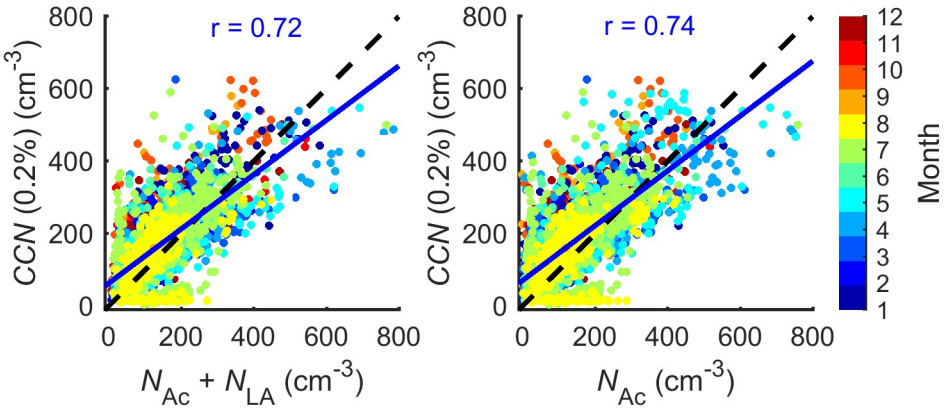

Figure S6. Comparison of observed *CCN* concentrations with relevant modal number concentrations. The black dash line is the 1:1 line shown for reference. The value of *r* given referred to the Pearson correlation coefficient, while the regression line based on York et al. (2004) is also shown for reference.

References

Anderson, T. L., and Ogren, J. A.: Determining Aerosol Radiative Properties Using the TSI 3563 Integrating Nephelometer, Aerosol Science and Technology, 29, 57-69, 10.1080/02786829808965551, 1998.

Bond, T. C., Anderson, T. L., and Campbell, D.: Calibration and Intercomparison of Filter-Based Measurements of Visible Light Absorption by Aerosols, Aerosol Science and Technology, 30, 582-600, 10.1080/027868299304435, 1999.

Costabile, F., Barnaba, F., Angelini, F., and Gobbi, G. P.: Identification of key aerosol populations through their size and composition resolved spectral scattering and absorption, Atmos. Chem. Phys., 13, 2455-2470, 10.5194/acp-13-2455-2013, 2013.

Langley, L., Leaitch, W. R., Lohmann, U., Shantz, N. C., and Worsnop, D. R.: Contributions from DMS and ship emissions to CCN observed over the summertime North Pacific, Atmos. Chem. Phys., 10, 1287-1314, 10.5194/acp-10-1287-2010, 2010.

Müller, T., Laborde, M., Kassell, G., and Wiedensohler, A.: Design and performance of a three-wavelength LED-based total scatter and backscatter integrating nephelometer, Atmos. Meas. Tech., 4, 1291-1303, 10.5194/amt-4-1291-2011, 2011.

Virkkula, A., Ahlquist, N. C., Covert, D. S., Arnott, W. P., Sheridan, P. J., Quinn, P. K., and Coffman, D. J.: Modification, Calibration and a Field Test of an Instrument for Measuring Light Absorption by Particles, Aerosol Science and Technology, 39, 68-83, 10.1080/027868290901963, 2005.

Virkkula, A.: Correction of the Calibration of the 3-wavelength Particle Soot Absorption Photometer (3λ PSAP), Aerosol Science and Technology, 44, 706-712, 10.1080/02786826.2010.482110, 2010.

Wood, R., Wyant, M., Bretherton, C. S., Rémillard, J., Kollias, P., Fletcher, J., Stemmler, J., Szoeke, S. d., Yuter, S., Miller, M., Mechem, D., Tselioudis, G., Chiu, J. C., Mann, J. A. L., O'Connor, E. J., Hogan, R. J., Dong, X., Miller, M., Ghate, V., Jefferson, A., Min, Q., Minnis, P., Palikonda, R., Albrecht, B., Luke, E., Hannay, C., and Lin, Y.: Clouds, Aerosols, and Precipitation in the Marine Boundary Layer: An Arm Mobile Facility Deployment, Bulletin of the American Meteorological Society, 96, 419-440, 10.1175/bams-d-13-00180.1, 2015.

York, D., Evensen, N. M., Martınez, M. L., and De Basabe Delgado, J.: Unified equations for the slope, intercept, and standard errors of the best straight line, American Journal of Physics, 72, 367-375, 2004.

Zheng, G., Duan, F., Ma, Y., Zhang, Q., Huang, T., Kimoto, T., Cheng, Y., Su, H., and He, K.: Episode-Based Evolution Pattern Analysis of Haze Pollution: Method Development and Results from Beijing, China, Environmental Science & Technology, 50, 4632-4641, 10.1021/acs.est.5b05593, 2016.